PHYSICAL REVIEW D **83,** 074505 (2011)

Lattice results for low moments of light meson distribution amplitudes

R. Arthur,[1,*] P. A. Boyle,[1,†] D. Brömmel,[2,‡] M. A. Donnellan,[3,§] J. M. Flynn,[2,‖]
A. Jüttner,[4,¶] T. D. Rae,[2,**] and C. T. C. Sachrajda[2,††]

(RBC and UKQCD Collaborations)

[1]*SUPA, School of Physics, The University of Edinburgh, Edinburgh EH9 3JZ, United Kingdom*
[2]*School of Physics and Astronomy, University of Southampton, Southampton SO17 1BJ, United Kingdom*
[3]*NIC/DESY Zeuthen, Platanenallee 6, 15738 Zeuthen, Germany*
[4]*CERN, Physics Department, 1211 Geneva 23, Switzerland*
(Received 7 December 2010; published 12 April 2011)

As part of the UKQCD and RBC collaborations' $N_f = 2 + 1$ domain-wall fermion phenomenology programme, we calculate the first two moments of the light-cone distribution amplitudes of the pseudoscalar mesons π and K and the (longitudinally polarized) vector mesons ρ, K^*, and ϕ. We obtain the desired quantities with good precision and are able to discern the expected quark-mass dependence of SU(3)-flavor breaking effects. An important ingredient of the calculation is the nonperturbative renormalization of lattice operators using a regularization-independent momentum scheme.

DOI: 10.1103/PhysRevD.83.074505 PACS numbers: 12.38.Gc, 11.15.Ha

I. INTRODUCTION

Light-cone distribution amplitudes (DAs) are important nonperturbative quantities which (within the framework of collinear factorization) parametrize in partonic terms the components of the hadronic wave function that control hard exclusive processes. Such processes provide hadron structure information complementary to that obtained from hard inclusive reactions.

The structure functions for inclusive processes are more accessible both experimentally and theoretically, owing to their larger cross sections and branching ratios, simpler final-state detection, and more straightforward factorization properties. They do not specify the phases and correlations which would constitute amplitude-level hadron structure information, but probe instead the bound states' partonic content. Deep-inelastic scattering processes, for example, are controlled by the charge and momentum of the struck parton and are insensitive to its relation to the other hadronic constituents. The associated parton distribution functions (PDFs) are therefore single-particle probabilities, which reveal nothing about the role of particular Fock states or of correlations between quarks and gluons.

Distribution amplitudes, involved in exclusive processes, always appear in convolutions and, unlike the PDFs, are not directly measurable. These exclusive processes are dominated by specific partonic configurations. The outgoing quarks and gluons are unlikely to form a given final-state hadron unless they are approximately collinear with small transverse separation, or one of the partons carries almost all of the hadron's momentum (the soft overlap or Feynman mechanism). In the former case, the basis for collinear factorization [1], hard gluon exchange must occur to allow the struck or decaying parton to communicate with the others, turning them to the final direction. Since more partons require more hard gluons, exclusive cross sections and decay rates are dominated by the valence Fock state at leading order in Q^2, up to soft effects.

Hard exclusive processes are therefore controlled at leading order by the distribution amplitudes of leading twist (an operator's twist is the difference between its dimension and its spin): essentially the overlap of the hadronic state with the valence Fock state in which, for a meson, the collinear quark-antiquark pair has small transverse separation and carries longitudinal momentum fractions u and $\bar{u} = 1 - u$. The pion's electromagnetic form factor at large Q^2, for example, can be written as a convolution of distribution amplitudes $\phi_\pi(u, Q^2)$ for the incoming and outgoing pions with a perturbatively calculable hard-scattering kernel. Higher-twist DAs associated with power-suppressed contributions originate in, for example, higher Fock states [2]. We consider only leading, twist-2 DAs in this paper.

The phenomenological importance of hard exclusive processes has grown since collinear factorization was first established for cases such as the pion's electromagnetic

*r.arthur@sms.ed.ac.uk
†paboyle@ph.ed.ac.uk
‡Current address: Jülich Supercomputing Centre, Institute for Advanced Simulation, Forschungszentrum Jülich GmbH, 52425 Jülich, Germany.
d.broemmel@fz-juelich.de
§michael.donnellan@desy.de
‖j.m.flynn@soton.ac.uk
¶juettner@mail.cern.ch
**t.d.rae@phys.soton.ac.uk
††cts@soton.ac.uk

form factor and the $\gamma\gamma^*\pi$ transition form factor around 30 years ago [1,3–5]. Of particular importance is the theoretical description of hadronic B decays, which have been studied in detail by *BABAR* and Belle and will be studied by LHCb and at super-B factories in order to constrain the Cabibbo-Kobayashi-Maskawa (CKM) matrix and to understand CP violation. Factorization is more difficult to establish in B physics because the hard-collinear and soft mechanisms contribute at the same order in $1/m_b$. Two approaches have been developed. In the QCD factorization framework it has been shown that collinear factorization can be applied to leading order in $1/m_b$ to a large class of nonleptonic B decays [6–8]. Soft-collinear effective theory (SCET) [9–11] aims to provide a unified theoretical framework for the factorization of both hard-collinear and soft effects. In both cases, distribution amplitudes play an important role as nonperturbative inputs in flavor physics.

In this paper we focus on the distribution amplitudes of the light pseudoscalar and longitudinally polarized vector mesons, since, as we shall discuss in Sec. I B, their lowest moments are of phenomenological interest and are calculable on the lattice. For pseudoscalars, these quantities are relevant for decays such as $B \to \pi\pi$ and $B \to \pi K$; they also appear in light-cone sum rule (LCSR) expressions for the form factors of semileptonic decays such as $B \to \pi l \nu$. For hard exclusive processes involving the light vector mesons ρ, K^*, and ϕ, polarization dependence can reveal much about the underlying dynamics, with the longitudinally and transversely polarized final vector meson states often involving different aspects of weak interaction physics [12]. Examples are the exclusive semileptonic $B \to \rho l \nu_l$, rare radiative $B \to \rho\gamma$, or nonleptonic, e.g. $B \to \pi\rho$, decays of B mesons, which are important for extracting CKM matrix elements.

A. Definitions

Mesonic light-cone DAs are defined from meson-to-vacuum matrix elements of quark-antiquark light-cone operators, which are nonlocal generalizations of those used to define the decay constants. For example, for pions

$$\begin{aligned}&\langle 0|\bar{q}_2(z)\gamma_\nu\gamma_5 P(z,-z)q_1(-z)|\pi(p)\rangle_{z^2=0}\\ &\quad\equiv if_\pi p_\nu \int_0^1 du e^{i(u-\bar{u})p\cdot z}\phi_\pi(u,\mu)\end{aligned} \tag{1}$$

and for longitudinally polarized rho mesons

$$\begin{aligned}&\langle 0|\bar{q}_2(z)\gamma_\nu P(z,-z)q_1(-z)|\rho(p;\lambda)\rangle_{z^2=0}\\ &\quad\equiv f_\rho m_\rho p_\nu \frac{\varepsilon(\lambda)\cdot z}{p\cdot z}\int_0^1 du e^{i(u-\bar{u})p.z}\phi_\rho^{\parallel}(u,\mu),\end{aligned} \tag{2}$$

where

$$\mathcal{P}(z,-z) = \mathcal{P}\exp\left(-ig\int_{-z}^{z} dw^\mu A_\mu(w)\right) \tag{3}$$

is the path-ordered exponential needed to maintain gauge invariance, μ is a renormalization scale, u is the momentum fraction of a quark, $\bar{u} = 1 - u$, and $\varepsilon^{(\lambda)}$ is the polarization vector for a vector meson with polarization state λ. The distribution amplitudes are normalized by

$$\int_0^1 du\phi(u,\mu) = 1. \tag{4}$$

The definitions above involve the pion and rho-meson decay constants defined by

$$\langle 0|\bar{q}_2\gamma_\mu\gamma_5 q_1|\pi(p)\rangle = if_\pi p_\mu, \tag{5}$$

$$\langle 0|\bar{q}_2\gamma_\mu q_1|\rho(p;\lambda)\rangle = f_\rho m_\rho \varepsilon_\mu^{(\lambda)}. \tag{6}$$

The vector meson decay constant f_ρ and its coupling to the tensor current, f_ρ^T, are of interest in their own right, and we have previously calculated [13] the ratios f_V^T/f_V, for $V \in \{\rho, K^*, \phi\}$, as part of our domain-wall fermion (DWF) phenomenology programme.

B. Moments

Moments of light-cone DAs are defined by

$$\langle \xi^n\rangle_\pi(\mu) = \int_0^1 du \xi^n \phi(u,\mu), \tag{7}$$

where $\xi \equiv u - \bar{u} = 2u - 1$ is the difference between the longitudinal momentum fractions.

Since the moments are obtained from matrix elements of local operators [14], we can study them using lattice QCD. The light-cone matrix elements which define the DAs themselves are not amenable to standard lattice techniques, since in Euclidean space the light cone has been rotated to the complex direction. By expanding the nonlocal operators on the light cone, we obtain symmetric, traceless twist-2 operators. With the following conventions for continuum covariant derivatives,

$$\begin{aligned}\vec{D}_\mu &= \vec{\partial}_\mu + igA_\mu,\\ \overleftarrow{D}_\mu &= \overleftarrow{\partial}_\mu - igA_\mu,\\ \overleftrightarrow{D}_\mu &= \overleftarrow{D}_\mu - \vec{D}_\mu,\end{aligned} \tag{8}$$

the expressions relating the moments of DAs to the corresponding local matrix elements are

$$\langle 0|\bar{q}(0)\gamma_\rho\gamma_5\overleftrightarrow{D}_\mu s(0)|K(p)\rangle = \langle\xi^1\rangle_K f_K p_\rho p_\mu, \tag{9a}$$

$$\langle 0|\bar{q}(0)\gamma_\rho\gamma_5\overleftrightarrow{D}_\mu\overleftrightarrow{D}_\nu q(0)|\pi(p)\rangle = -i\langle\xi^2\rangle_\pi f_\pi p_\rho p_\mu p_\nu, \tag{9b}$$

$$\langle 0|\bar{q}(0)\gamma_\rho\overleftrightarrow{D}_\mu s(0)|K^*(p,\lambda)\rangle = \langle\xi^1\rangle^{\parallel}_{K^*} f_{K^*} m_{K^*}\tfrac{1}{2}(p_\mu\varepsilon^{(\lambda)}_\nu + p_\nu\varepsilon^{(\lambda)}_\mu), \tag{9c}$$

$$\langle 0|\bar{q}(0)\gamma_\rho\overleftrightarrow{D}_\mu\overleftrightarrow{D}_\nu q(0)|\rho(p,\lambda)\rangle = -i\langle\xi^2\rangle^{\parallel}_\rho f_\rho m_\rho\tfrac{1}{3}(\varepsilon^{(\lambda)}_\rho p_\mu p_\nu + \varepsilon^{(\lambda)}_\mu p_\nu p_\rho + \varepsilon^{(\lambda)}_\nu p_\rho p_\mu). \tag{9d}$$

The operators in the matrix elements above are all to be considered symmetric and traceless in the free Lorentz indices. Meson-meson rather than meson-vacuum matrix elements of the same operators lead to moments of generalized parton distributions (GPDs).

Recent analyses, especially those based on QCD sum rules, deal instead with the Gegenbauer moments, which arise from a conformal expansion [15,16], in which the conformal invariance of (classical) massless QCD is used to separate longitudinal and transverse degrees of freedom, analogous to the partial wave expansion in ordinary quantum mechanics. All dependence on the longitudinal momentum fractions is described by orthogonal polynomials that form an irreducible representation of the collinear subgroup of the conformal group, $\mathrm{SL}(2,\mathbb{R})$. The transverse-momentum dependence is represented as the scale dependence of the relevant operators and is governed by renormalization-group equations. The different ''partial waves,'' labeled by different conformal spins, do mix but not to leading-logarithmic accuracy. Conformal spin is thus a good quantum number in hard processes up to small corrections of order α_s^2.

The asymptotic $Q^2 \to \infty$ DA is known from perturbative QCD: $\phi_{\mathrm{as}} = 6u\bar{u}$. For the leading-twist quark-antiquark DAs that we are interested in, the conformal expansion can then be conveniently written as

$$\phi(u,\mu) = 6u\bar{u}\Big(1 + \sum_{n=1}^{\infty} a_n(\mu)C_n^{3/2}(2u-1)\Big), \tag{10}$$

where $C_n^{3/2}$ are Gegenbauer polynomials. To one-loop order the Gegenbauer moments a_n renormalize multiplicatively [16]:

$$a_n(\mu) = a_n(\mu_0)\Big(\frac{\alpha_s(\mu)}{\alpha_s(\mu_0)}\Big)^{(\gamma_{(n)}-\gamma_{(0)})/\beta_0}. \tag{11}$$

The one-loop anomalous dimensions are

$$\gamma_{(n)} = \gamma^{\parallel}_{(n)} = C_F\Big(1 - \frac{2}{(n+1)(n+2)} + 4\sum_{j=2}^{n+1} 1/j\Big), \tag{12}$$

where $C_F = 4/3$. Since the moments are positive and increase with n, the effects of higher-order Gegenbauer polynomials are damped at higher scales as the DAs approach their asymptotic form. The conformal expansion can thus be truncated. Quantities such as the pion's electromagnetic form factor, for example, are given by convolutions in which the kernels are slowly varying and the strongly oscillating Gegenbauer polynomials are washed out. The same conclusion is reached by considering, rather than the conformal expansion, the diagonalization of the Efremov-Radyushkin-Brodsky-Lepage equations [1,4,17,18] which govern the evolution of the DAs much as the Dokshitzer-Gribov-Lipatov-Altarelli-Parisi equations [19–22] govern the evolution of PDFs.

We can obtain values for the Gegenbauer moments from lattice simulations since the Gegenbauer moments are combinations of ordinary moments of equal and lower order, e.g.

$$a_1 = \frac{5}{3}\langle\xi^1\rangle, \qquad a_2 = \frac{7}{12}(5\langle\xi^2\rangle - 1). \tag{13}$$

C. Status

In this section, we summarize what is currently known about leading-twist light-meson distribution amplitudes. For mesons of definite G parity, there is a symmetry under the interchange $u \leftrightarrow \bar{u}$ of the two momentum fractions. In these cases, the distribution amplitude is an even function of $\xi = u - \bar{u}$ and the odd moments therefore vanish. Thus, $\langle\xi^1\rangle_\pi$, $\langle\xi^1\rangle^{\parallel}_\rho$, and $\langle\xi^1\rangle^{\parallel}_\phi$ all vanish, while $\langle\xi^1\rangle_K$ and $\langle\xi^1\rangle^{\parallel}_{K^*}$ are SU(3)-flavor breaking effects.

Since $\langle\xi^1\rangle_K$ is the average difference between the fractions of longitudinal momentum carried by the strange and light quarks,

$$\langle\xi^1\rangle_K(\mu) = \int_0^1 du(2u-1)\phi_K(u,\mu) = \langle 2u-1\rangle, \tag{14}$$

we may expect from the constituent quark model that the sign of $\langle\xi^1\rangle_K = \frac{3}{5}a_1^K$ is positive, and this is indeed the case. In fact, $\langle\xi^1\rangle_K$ is an important SU(3)-breaking parameter and is relevant for predictions of B-decay transitions such as $B \to K$, K^* [23]. For example, a light-cone sum rule analysis leads to [24]

$$\frac{f_+^{BK}(0)}{f_+^{B\pi}(0)} = \frac{f_K}{f_\pi}(1 + c_1 a_1^K) + \ldots, \tag{15}$$

where $f_+^{BP}(0)$ is the vector $B \to P$ form factor at zero momentum transfer and $c_1 \sim O(1)$. Other examples include the ratio of the weak radiative decay amplitudes $B \to \rho\gamma$ and $B \to K^*\gamma$, where the main theoretical error originates from such SU(3)-breaking effects. The measured ratio of these decay rates allows for the determination of the ratio of CKM matrix elements $|V_{ts}|/|V_{td}|$.

There have been three main approaches to the study of DAs: extraction from experimental data, calculations using QCD sum rules, and lattice calculations. The overall normalizations are given by local hadronic matrix elements, essentially the decay constants, which have already been discussed and are partly accessible experimentally, and partly have to be calculated theoretically. The shapes of the leading-twist distribution amplitudes, in the form of the Gegenbauer moments, can be determined from experiments by analyzing data on form factors such as $F_{\gamma\gamma^*\pi}$, which was studied by the CLEO experiment [25], and the pion's electromagnetic form factor, $F_\pi^{\rm em}$ [26]. There is a lack of sufficiently accurate data, however, and it is difficult to avoid contamination from other hadronic uncertainties and higher-twist effects. As a result, the existing experimental constraints are not very stringent.

Moments of DAs, then, must largely be determined from theory. Lattice [23,27–32] and sum rule [33–36] studies have usually focused on the second moment of the pion's distribution amplitude. However, the early lattice results were largely exploratory while sum rule results have an irreducible error of $\sim$20% because it is not possible to properly isolate the hadronic states.

The first moment of the kaon's distribution amplitude, for example, has, in the past, been determined mainly from QCD sum rules, and representative results include

$$a_1^K(1\ \text{GeV}) = \begin{cases} 0.05(2) & [37] \\ 0.10(12) & [38] \\ 0.050(25) & [39] \\ 0.06(3) & [40]. \end{cases} \tag{16}$$

These results all have the expected sign, but the uncertainties are around 50%. The reduction of such uncertainties is the chief motivation of the lattice programme. In an earlier publication [41,42], we obtained $\langle\xi^1\rangle_K(2\ \text{GeV}) \equiv 3/5a_K^1(2\ \text{GeV}) = 0.032(3)$. We note that in addition to the UKQCD/RBC programme for the calculation of DA moments on the lattice using $N_f = 2 + 1$ domain-wall fermions, there is a UKQCD/QCDSF programme using $N_f = 2$ improved Wilson quarks [23]. QCDSF have also published results for moments of baryon DAs [28]. Lattice results for hadronic distribution amplitudes are considered in a recent review of hadron structure from lattice QCD in [43].

The plan for the remainder of this paper is as follows. In Sec. II we discuss the extraction of bare moments of distribution amplitudes from Euclidean lattice correlation functions (we use "bare" or "latt" to denote quantities before matching from the lattice to the continuum). In Sec. III we give the details of our numerical calculations and present the bare results. The renormalization of those bare results is described in Sec. IV. We then present our summary in Sec. V.

II. BARE MOMENTS FROM LATTICE CORRELATION FUNCTIONS

In this section, we describe our general strategy for the lattice calculation of the unrenormalized lowest moments of light-meson distribution amplitudes. We obtain expressions for the first and second moments $\langle\xi^1\rangle$ and $\langle\xi^2\rangle$ for pseudoscalar mesons and for the longitudinal moments $\langle\xi^1\rangle^\parallel$ and $\langle\xi^2\rangle^\parallel$ for vector mesons, in terms of Euclidean lattice correlation functions which can be computed by Monte Carlo integration of the QCD path integral. In each case, we consider a generic meson having valence quark content $\bar{q}_2 q_1$, where the subscripts indicate that the flavors of the two quarks may be different. We will see below that we can obtain all of these moments from ratios of two-point correlation functions, and thus we expect to benefit from a significant reduction of the statistical fluctuations.

A. Lattice operators

We now define the lattice operators used in the correlation functions from which we extract the moments of the distribution amplitudes. We use the following interpolating operators for the pseudoscalar and vector mesons:

$$P(x) \equiv \bar{q}_2(x)\gamma_5 q_1(x), \tag{17a}$$

$$V_\mu(x) \equiv \bar{q}_2(x)\gamma_\mu q_1(x), \tag{17b}$$

$$A_\mu(x) \equiv \bar{q}_2(x)\gamma_\mu\gamma_5 q_1(x). \tag{17c}$$

Although we have written P, V, and A as local operators in Eq. (17), in the numerical simulations we use smeared operators at the source of our correlation functions in order to improve the overlap with the lightest meson states. Since the effects of smearing cancel in the ratios constructed below, the discussion in this section holds for both smeared and local interpolating operators. We explain the details of our smearing procedures in Sec. III A. The operators in Eqs. (9) from which the moments of the distribution amplitudes are obtained are of course local operators.

In constructing the lattice operators of Eqs. (9), we use the following symmetric left- and right-acting covariant derivatives:

$$\vec{D}_\mu\psi(x) = \frac{1}{2a}[U(x, x+\hat{\mu})\psi(x+\hat{\mu}) - U(x, x-\hat{\mu})\psi(x-\hat{\mu})], \tag{18}$$

$$\bar{\psi}(x)\overleftarrow{D}_\mu = \frac{1}{2a}[\bar{\psi}(x+\hat{\mu})U(x+\hat{\mu}, x) - \bar{\psi}(x-\hat{\mu})U(x-\hat{\mu}, x)], \tag{19}$$

where $U(x, y)$ is the gauge link going from site x to site y, and $\hat{\mu}$ is a vector of length a in the direction μ (a denotes the lattice spacing). The operators of interest are then defined by

$$\mathcal{O}_{\{\rho\mu\}}(x) \equiv \bar{q}_2(x)\gamma_{\{\rho}\overleftrightarrow{D}_{\mu\}}q_1(x), \tag{20a}$$

$$\mathcal{O}_{\{\rho\mu\nu\}}(x) \equiv \bar{q}_2(x)\gamma_{\{\rho}\overleftrightarrow{D}_{\mu}\overleftrightarrow{D}_{\nu\}}q_1(x), \tag{20b}$$

$$\mathcal{O}^5_{\{\rho\mu\}}(x) \equiv \bar{q}_2(x)\gamma_{\{\rho}\gamma_5\overleftrightarrow{D}_{\mu\}}q_1(x), \tag{20c}$$

$$\mathcal{O}^5_{\{\rho\mu\nu\}}(x) \equiv \bar{q}_2(x)\gamma_{\{\rho}\gamma_5\overleftrightarrow{D}_{\mu}\overleftrightarrow{D}_{\nu}D_{\nu\}}q_1(x), \tag{20d}$$

where the braces in the subscripts indicate symmetrization of the enclosed Lorentz indices, $\{\mu_1 \ldots \mu_n\} \equiv \sum_{\text{perms}\,s}\{\mu_{s(1)} \ldots \mu_{s(n)}\}/n!$.

B. Operator mixing

In the continuum the operators in Eq. (20) transform as second- or third-rank tensors under the Lorentz group. On the lattice, however, we must consider their transformation properties under the hypercubic group $\mathcal{H}_4$ of reflections and $\pi/2$ rotations, together with the discrete symmetries parity P and charge-conjugation C, where the possibilities for operator mixing are increased. A detailed study of the transformations of these operators under $\mathcal{H}_4$ has been performed in [44].

The choice of Lorentz indices in the operators used in simulations is important both to keep the operator mixing simple and also to enable the extraction of matrix elements using as few nonzero components of momentum as possible. The latter is to avoid the associated discretization effects and statistical degradation. $\mathcal{O}_{\{\rho\mu\}}$ and $\mathcal{O}^5_{\{\rho\mu\}}$ renormalize multiplicatively under $\mathcal{H}_4$ when $\rho \neq \mu$. In the notation of [45], these operators transform under the six-dimensional $6^{(+)}$ (for $\mathcal{O}^5_{\{\rho\mu\}}$) or $6^{(-)}$ (for $\mathcal{O}_{\{\rho\mu\}}$) irreducible representations of $\mathcal{H}_4$. The choice $\mu \neq \rho$ is the most convenient one for the extraction of the first moment of the distribution amplitudes. Charge-conjugation symmetry combined with $\mathcal{H}_4$ ensures that there is no mixing with operators containing total derivatives.

It is also possible to obtain the first moment from the four operators $\mathcal{O}_{\{\mu\mu\}}$ (or $\mathcal{O}^5_{\{\mu\mu\}}$), which each transform as four-dimensional reducible representations containing a singlet. The three traceless operators transform as the three-dimensional irreducible representation $(3, 1)^{(+)}$ (without γ^5) or $(3, 1)^{(-)}$ (with γ^5). Subtracting the trace involves the subtraction of a power divergence, so for the first moment of the distribution amplitude of the K and K^*, we avoid this by evaluating the matrix elements of $\mathcal{O}^5_{\{\rho\mu\}}$ and $\mathcal{O}_{\{\rho\mu\}}$, respectively, with $\rho \neq \mu$.

Similarly, for the second moment of the distribution amplitudes the most convenient choice is to use $\mathcal{O}^5_{\{\rho\mu\nu\}}$ or $\mathcal{O}_{\{\rho\mu\nu\}}$ with all three indices different, which transform as the $\overline{(1/2, 1/2)}^{(+)}$ and $\overline{(1/2, 1/2)}^{(-)}$ four-dimensional irreducible representations, respectively. Charge-conjugation symmetry allows mixing of $\mathcal{O}^5_{\{\rho\mu\nu\}}$ and $\mathcal{O}_{\{\rho\mu\nu\}}$ with operators containing total derivatives:

$\mathcal{O}^5_{\{\rho\mu\nu\}}(x)$ mixes with $\partial_{\{\rho}\partial_\mu(\bar{q}_2(x)\gamma_{\nu\}}\gamma_5 q_1(x))$,

$\mathcal{O}_{\{\rho\mu\nu\}}(x)$ mixes with $\partial_{\{\rho}\partial_\mu(\bar{q}_2(x)\gamma_{\nu\}}q_1(x))$.

The moments of the distribution functions are obtained from nonforward matrix elements between a meson at nonzero four-momentum and the vacuum, so the total-derivative operators must be included in the analysis.

C. $\langle \xi^1 \rangle_P$ and $\langle \xi^2 \rangle_P$ from correlation function ratios

To obtain the first and second moments of the pseudoscalar meson distribution amplitude, $\langle \xi^1 \rangle$ and $\langle \xi^2 \rangle$, we consider the following two-point correlation functions:

$$C_{A_\nu P}(t, \boldsymbol{p}) \equiv \sum_{\boldsymbol{x}} e^{i\boldsymbol{p}\cdot\boldsymbol{x}}\langle 0|A_\nu(t, \boldsymbol{x})P^\dagger(0)|0\rangle, \tag{21a}$$

$$C^5_{\{\rho\mu\}}(t, \boldsymbol{p}) \equiv \sum_{\boldsymbol{x}} e^{i\boldsymbol{p}\cdot\boldsymbol{x}}\langle 0|\mathcal{O}^5_{\{\rho\mu\}}(t, \boldsymbol{x})P^\dagger(0)|0\rangle, \tag{21b}$$

$$C^5_{\{\rho\mu\nu\}}(t, \boldsymbol{p}) \equiv \sum_{\boldsymbol{x}} e^{i\boldsymbol{p}\cdot\boldsymbol{x}}\langle 0|\mathcal{O}^5_{\{\rho\mu\nu\}}(t, \boldsymbol{x})P^\dagger(0)|0\rangle. \tag{21c}$$

For a generic pseudoscalar meson P, we define $Z_P \equiv \langle P(p)|P^\dagger|0\rangle$ and the bare decay constant by $\langle 0|A_\nu|P(p)\rangle \equiv ip_\nu f_P^{\text{bare}}$. The operators $P^\dagger(0)$ in Eqs. (21) are smeared, as explained below. At large Euclidean times t and $T - t$, the correlation functions defined above tend towards

$$C_{A_\nu P}(t, \boldsymbol{p}) \to \frac{Z_P f_P^{\text{bare}} e^{-E_P T/2}\sinh((t - T/2)E_P)}{E_P} ip_\nu, \tag{22}$$

$$C^5_{\{\rho\mu\}}(t, \boldsymbol{p}) \to \frac{Z_P f_P^{\text{bare}} e^{-E_P T/2}\sinh((t - T/2)E_P)}{E_P} \times ip_\rho ip_\mu \langle \xi^1 \rangle^{\text{bare}}, \tag{23}$$

$$C^5_{\{\rho\mu\nu\}}(t, \boldsymbol{p}) \to \frac{Z_P f_P^{\text{bare}} e^{-E_P T/2}\sinh((t - T/2)E_P)}{E_P} \times ip_\rho ip_\mu ip_\nu \langle \xi^2 \rangle^{\text{bare}}. \tag{24}$$

We can extract bare values for the first and second moments of the pseudoscalar meson distribution amplitudes from the following ratios of correlation functions:

$$R^P_{\{\rho\mu\};\nu}(t, \boldsymbol{p}) \equiv \frac{C^5_{\{\rho\mu\}}(t, \boldsymbol{p})}{C_{A_\nu P}(t, \boldsymbol{p})} \to i\frac{p_\rho p_\mu}{p_\nu}\langle \xi^1 \rangle^{\text{bare}}, \tag{25a}$$

$$R^P_{\{\rho\mu\nu\};\sigma}(t, \boldsymbol{p}) \equiv \frac{C^5_{\{\rho\mu\nu\}}(t, \boldsymbol{p})}{C_{A_\sigma P}(t, \boldsymbol{p})} \to -\frac{p_\rho p_\mu p_\nu}{p_\sigma}\langle \xi^2 \rangle^{\text{bare}}. \tag{25b}$$

Keeping in mind the operator mixing outlined above, we obtain the first moment from $R^P_{\{\rho 4\};4}(t, \boldsymbol{p})$ (the index 4

corresponds to the time direction) with $\rho = 1$, 2, or 3 and a single nonzero component of momentum, $|p_\rho| = 2\pi/L$. The second moment is extracted from $R^P_{\{\rho\mu 4\};4}(t, \boldsymbol{p})$ with at least two nonzero components of momentum. We take ρ, $\mu = 1$, 2, or 3 with $\rho \neq \mu$ and $|p_\rho| = |p_\mu| = 2\pi/L$. We present more details in Sec. III B.

Apart from isolating the moments of the DAs as much as possible by canceling Z_P, f_P^{bare}, and most of the energy dependence from Eqs. (23) and (24), the ratios also simplify the effect of mixing with total-derivative operators. These operators have matrix elements proportional to (22) with which we build a ratio similar to (25b). Hence the contribution of the mixing term becomes trivial and does not have to be computed explicitly. It enters as an additive constant when renormalizing the bare moments, as we will discuss later.

D. $\langle \xi^1 \rangle_V^{\parallel}$ and $\langle \xi^2 \rangle_V^{\parallel}$ from correlation function ratios

The treatment of the vector meson's longitudinal distribution amplitude is analogous. We consider the following two-point correlation functions:

$$C_{V_\mu V_\nu}(t, \boldsymbol{p}) \equiv \sum_{\boldsymbol{x}} e^{i\boldsymbol{p}\cdot\boldsymbol{x}} \langle 0 | V_\mu(t, \boldsymbol{x}) V_\nu^\dagger(0) | 0 \rangle, \tag{26a}$$

$$C_{\{\rho\mu\}\nu}(t, \boldsymbol{p}) \equiv \sum_{\boldsymbol{x}} e^{i\boldsymbol{p}\cdot\boldsymbol{x}} \langle 0 | \mathcal{O}_{\{\rho\mu\}}(t, \boldsymbol{x}) V_\nu^\dagger(0) | 0 \rangle, \tag{26b}$$

$$C_{\{\rho\mu\nu\}\sigma}(t, \boldsymbol{p}) \equiv \sum_{\boldsymbol{x}} e^{i\boldsymbol{p}\cdot\boldsymbol{x}} \langle 0 | \mathcal{O}_{\{\rho\mu\nu\}}(t, \boldsymbol{x}) V_\sigma^\dagger(0) | 0 \rangle. \tag{26c}$$

Again, the source operators $V^\dagger(0)$ are smeared. We define the bare longitudinal decay constant of a vector meson V, with polarization index λ and polarization vector $\varepsilon_\mu^{(\lambda)}$, by $\langle 0 | V_\mu | V(p, \lambda) \rangle \equiv f_V^{\text{bare}} m_V \varepsilon_\mu^{(\lambda)}$. Then, at large Euclidean times t and $T - t$, the correlation functions defined above may be written

$$C_{V_\mu V_\nu}(t, \boldsymbol{p}) \to \frac{-(f_V^{\text{bare}} m_V)^2 e^{-E_V T/2} \cosh((t - T/2)E_V)}{E_V} \left(-g_{\mu\nu} + \frac{p_\mu p_\nu}{m_V^2} \right), \tag{27a}$$

$$C_{\{\rho\mu\}\nu}(t, \boldsymbol{p}) \to \frac{-i(f_V^{\text{bare}} m_V)^2 e^{-E_V T/2} \langle \xi^1 \rangle^{\parallel \text{bare}} \sinh((t - T/2)E_V)}{E_V} \frac{1}{2} \left(-g_{\rho\nu} p_\mu - g_{\mu\nu} p_\rho + \frac{2 p_\rho p_\mu p_\nu}{m_V^2} \right), \tag{27b}$$

$$C_{\{\rho\mu\nu\}\sigma}(t, \boldsymbol{p}) \to \frac{(f_V^{\text{bare}} m_V)^2 e^{-E_V T/2} \langle \xi^2 \rangle^{\parallel \text{bare}} \sinh((t - T/2)E_V)}{E_V} \frac{1}{3} \left(-g_{\rho\sigma} p_\mu p_\nu - g_{\mu\sigma} p_\rho p_\nu - g_{\nu\sigma} p_\rho p_\mu + \frac{3 p_\rho p_\mu p_\nu p_\sigma}{m_V^2} \right), \tag{27c}$$

where we have used the completeness relation for the polarization vectors of massive vector particles, $\sum_\lambda \varepsilon_\mu^{(\lambda)} \varepsilon_\nu^{*(\lambda)} = -g_{\mu\nu} + p_\mu p_\nu / m_V^2$. We extract bare values for the first and second moments from the following ratios:

$$R^V_{\{\rho\mu\}\nu}(t, \boldsymbol{p}) \equiv \frac{C_{\{\rho\mu\}\nu}(t, \boldsymbol{p})}{\frac{1}{3}\sum_i C_{V_i V_i}(t, \boldsymbol{p} = 0)} \to -i \langle \xi^1 \rangle^{\parallel \text{bare}} \tanh((t - T/2)E_V) \frac{1}{2} \left(-g_{\rho\nu} p_\mu - g_{\mu\nu} p_\rho + \frac{2 p_\rho p_\mu p_\nu}{m_V^2} \right), \tag{28a}$$

$$R^V_{\{\rho\mu\nu\}\sigma}(t, \boldsymbol{p}) \equiv \frac{C_{\{\rho\mu\nu\}\sigma}(t, \boldsymbol{p})}{\frac{1}{3}\sum_i C_{V_i V_i}(t, p_i = 0, |\boldsymbol{p}| = \frac{2\pi}{L})} \to \langle \xi^2 \rangle^{\parallel \text{bare}} \tanh((t - T/2)E_V) \times \frac{1}{3} \left(-g_{\rho\sigma} p_\mu p_\nu - g_{\mu\sigma} p_\rho p_\nu - g_{\nu\sigma} p_\rho p_\mu + \frac{3 p_\rho p_\mu p_\nu p_\sigma}{m_V^2} \right), \tag{28b}$$

where the index i runs over spatial dimensions only. We obtain the first moment from $R^V_{\{\rho 4\}\nu}(t, \boldsymbol{p})$ at $\boldsymbol{p} = 0$ by taking $\rho = \nu = 1$, 2, or 3. The second moment is obtained from $R^V_{\{\rho\mu\nu\}\sigma}(t, \boldsymbol{p})$ by taking, for example, $\nu = 4$, $\rho = 1$, $\mu = \sigma = 2$, and a single nonzero component of $\boldsymbol{p}$ in the 1-direction.

III. NUMERICAL SIMULATIONS AND RESULTS

A. Simulation details

Our numerical calculations are based upon gauge field configurations drawn from the joint data sets used for the broader UKQCD/RBC domain-wall fermion phenomenology programme. Configurations were generated with $N_f = 2 + 1$ flavors of dynamical domain-wall fermions and with the Iwasaki gauge action, using the rational hybrid Monte Carlo (RHMC) [46] algorithm on QCDOC computers [47–49] running the Columbia Physics System (CPS) software [50] and the BAGEL [51,52] assembler generator.

Our set of gauge configurations includes data with two different volumes but at a single lattice spacing, thus giving us some indication of the size of finite volume effects but no ability to perform a continuum extrapolation. We

TABLE I. Lattice scale and unrenormalized quark masses in lattice units, from the 24^4 lattices [13]. Note $\tilde{m}_X \equiv m_X + m_{\rm res}$. Only the statistical errors are given here.

a^{-1} (GeV)	a (fm)	am_{ud}	$a\tilde{m}_{ud}$	am_s	$a\tilde{m}_s$	$a\tilde{m}_{ud}$:$a\tilde{m}_s$
1.729(28)	0.1141(18)	−0.001 847(58)	0.001 300(58)	0.034 3(16)	0.0375(16)	1:28.8(4)

therefore have an unavoidable systematic error which is, however, formally of $O(a^2\Lambda^2_{\rm QCD})$ due to the automatic $O(a)$ improvement of the DWF action and operators. In the future, this limitation will be overcome by performing the analysis with a data set with a finer lattice spacing with the same action. In the meantime, following the UKQCD/RBC procedure for these configurations [13], we ascribe a 4% uncertainty as the discretization error on the moments. For both volumes, we have a single dynamical strange-quark mass, close to its physical value. We use several independent ensembles with different light-quark masses ($m_u = m_d$), all heavier than those found in nature. The hadronic spectrum and other properties of these configurations have been studied in detail, and the results have been presented in [53] [for the lattice volume $(L/a)^3 \times T/a = 16^3 \times 32$] and [13] (for the lattice volume $24^3 \times 64$). In both cases the length of the fifth dimension is $L_s = 16$.

The choice of bare parameters in our simulations is $\beta = 2.13$ for the bare gauge coupling, $am_s = 0.04$ for the strange-quark mass, and $am_q = 0.03$, 0.02, 0.01, and, in the 24^3 case only, 0.005 for the bare light-quark masses. *A posteriori*, the strange-quark mass is found to be about 15% larger than its physical value. The lattice spacing is found to be $a^{-1} = 1.729(28)$ GeV [13], giving physical volumes of $(1.83\ {\rm fm})^3$ and $(2.74\ {\rm fm})^3$. The lattice spacing and physical quark masses were obtained using the masses of the π and K pseudoscalar mesons and the triply strange Ω baryon. The quark masses obtained in the 24^3 study are shown in Table I. Owing to the remnant chiral symmetry breaking, the quark mass has to be corrected additively by the residual mass in the chiral limit, $am_{\rm res} = 0.003\,15(2)$ [13]. The physical pion masses are as follows:

$$m_\pi \simeq \begin{cases} 670\ {\rm MeV} & am_q = 0.03 \\ 555\ {\rm MeV} & am_q = 0.02 \\ 415\ {\rm MeV} & am_q = 0.01 \\ 330\ {\rm MeV} & am_q = 0.005. \end{cases} \quad (29)$$

Measurements were performed using the UKHADRON software package that makes use of both the BAGEL DWF inverter [51,52] and elements of the SciDAC software library stack, including the CHROMA LQCD library [54] and QDP++. The details are summarized in Tables II and III. We restrict our analysis to the unitary data for which the valence- and sea-quark masses are the same (partially quenched data were used extensively in the studies of the chiral behavior of the spectrum and decay constants in [13]). On the 16^3 lattice, our data set differs from that used in [53] in that the Markov chains have been extended for the heaviest light-quark mass to give additional statistics, using an improved algorithm that decorrelated topology rather more quickly.

In order to improve the statistical sampling of the correlation functions, on each configuration we have averaged the results obtained from either two, three, or four sources spaced out along a lattice diagonal. In the 16^3 case, for example, the sources used are at the origin, at (4, 4, 4, 8), (8, 8, 8, 16), and (12, 12, 12, 24). Statistical errors for observables are estimated using single-elimination jackknife, with measurements made on the same configuration but at different source positions put in the same jackknife bin because of the correlations expected between them. In order to lessen the effect of autocorrelations, we follow the same blocking procedures as in [13,53]. In the 16^3 case, the span of the measurements in each block covers 50 molecular dynamics time units. In the 24^3 case, for the $m_q a = 0.005$ and $am_q = 0.01$ ensembles, each jackknife bin contains measurements from every 80 molecular dynamics time units, while for the $am_q = 0.02$ and $am_q = 0.03$

TABLE II. Parameters for our 16^3 data set, which corresponds largely to that of [53]. The range and measurement separation Δ are specified in molecular dynamics time units. $N_{\rm meas}$ is the number of measurements for each source position $t_{\rm src}$. The total number of measurements is therefore $N_{\rm meas} \times N_{\rm src}$, where $N_{\rm src}$ is the number of different values for $t_{\rm src}$. In the rightmost column, XY-XY denotes contraction of two quark propagators with X-type smearing at source and Y-type smearing at sink: G = Gaussian wave function, L = point.

m_l	Range	Δ	$N_{\rm meas}$	$t_{\rm src}$ locations	Smearing
0.01	500–3990	10	350	0, 8, 16, 24	GL-GL
0.02	500–3990	10	350	0, 8, 16, 24	GL-GL
0.03	4030–7600	10	358	0, 16	GL-GL

TABLE III. Parameters for our 24^3 data set, which corresponds to the unitary part of the data set of [13]. Columns are the same as in Table II, with the addition of H = gauge-fixed hydrogen S-wave smearing.

m_l	Range	Δ	$N_{\rm meas}$	$t_{\rm src}$ locations	Smearing
0.005	900–4480	20	180	0, 32, 16	HL-HL
0.01	800–3940	10	315	0, 2	GL-GL
0.02	1800–3580	20	90	0, 32	HL-HL
0.03	1260–3040	20	90	0, 32	HL-HL

ensembles, each bin contains measurements from every 40 molecular dynamics time units in order to have a reasonable number of bins for the analysis.

We use source smearing to improve the overlap with the mesonic states, either gauge-fixed hydrogen S-wavefunction smearing [55] with radius $r = 3.5$ in lattice units or gauge invariant Gaussian smearing [56] with radius $r = 4$.

B. Results

In order to extract $\langle \xi^1 \rangle_K$ from the ratio $R^P_{\{\rho\mu\};\nu}(t, \boldsymbol{p})$ defined in (25a), we need the two correlation functions to be measured at $|\boldsymbol{p}| \neq 0$. Since we expect hadronic observables with larger lattice momenta to have larger lattice artefacts and statistical errors, we restrict the choice of indices to $\rho = \nu = 4$ and $\mu = 1$, 2, or 3, with $|\boldsymbol{p}| = 2\pi/L$ (i.e., $p_\mu = \pm 2\pi/L$, with the remaining two components of $\boldsymbol{p}$ equal to 0). $\langle \xi^1 \rangle^{\text{bare}}_K$ can then be obtained from the ratio at large times:

$$R^P_{\{4k\};4}(t, p_k = \pm 2\pi/L) = \pm i \frac{2\pi}{L} \langle \xi^1 \rangle^{\text{bare}}, \qquad (30)$$

with $|\boldsymbol{p}| = 2\pi/L$ and $k = 1, 2, 3$. The plots in Fig. 1 show our results for $\langle \xi^1 \rangle^{\text{bare}}_K$ as a function of t obtained from the ratio $R^P_{\{4k\};4}(t, p_k = \pm 2\pi/L)$ for the four values of the light-quark mass, combining results at t with those at $T - t - 1$. The results have been averaged over the three values of k and, in total, the six equivalent lattice momenta with $|\boldsymbol{p}| = 2\pi/L$.

To obtain $\langle \xi^2 \rangle^{\text{bare}}_{\pi,K}$ from the ratio $R^P_{\{\rho\mu\nu\};\sigma}(t, \boldsymbol{p})$ defined in (25b), we need two nonzero components of momentum, so we use

$$R^P_{\{4jk\};4}(t, pj = \pm 2\pi/L, pk = \pm 2\pi/L) = -\left(\pm \frac{2\pi}{L}\right)\left(\pm \frac{2\pi}{L}\right) \langle \xi 2 \rangle^{\text{bare}} \qquad (31)$$

with $|\boldsymbol{p}| = \sqrt{2}2\pi/L$, $k, j = 1, 2, 3$ and $k \neq j$. We average over all four momentum combinations appropriate to each of the three possible Lorentz index choices.

We may extract $\langle \xi^1 \rangle^{\|\text{bare}}_{K^*}$ from the ratio $R^V_{\{\rho\mu\}\nu}(t, \boldsymbol{p})$ defined in (28a) by considering only zero-momentum correlation functions. In the denominator, we average

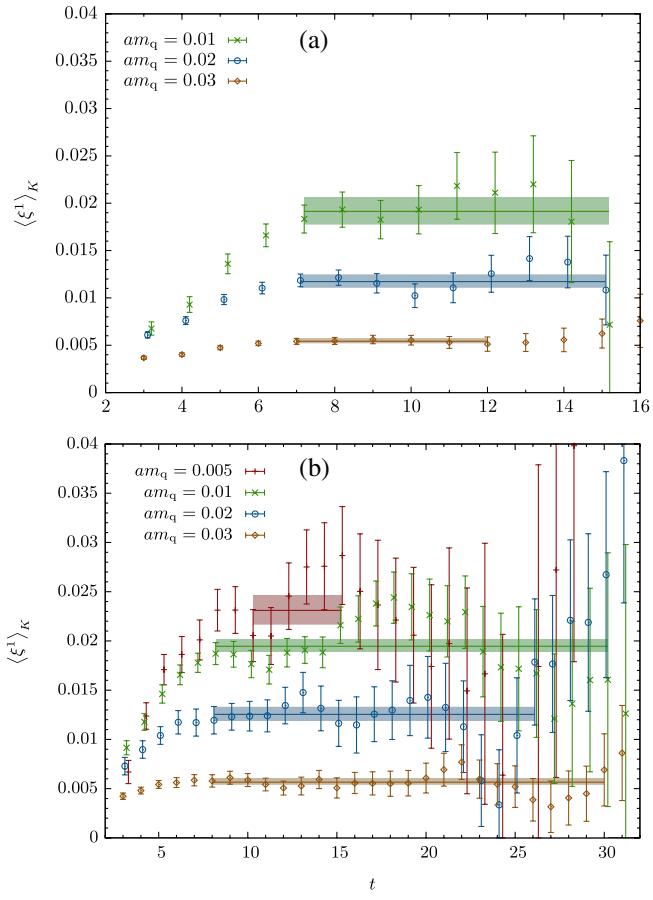

FIG. 1 (color online). Results for $\langle \xi^1 \rangle^{\text{bare}}_K$ as a function of time, on the 16^3 (top panel) and 24^3 (bottom panel) lattices. The shaded band shows the fit range, and the fitted value and its error.

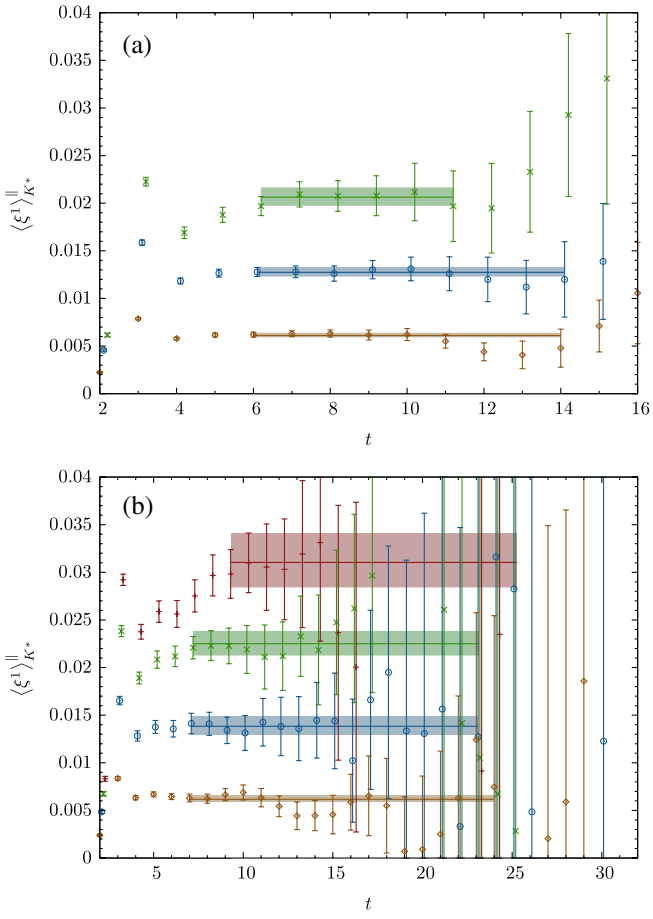

FIG. 2 (color online). Results for $\langle \xi^1 \rangle^{\|\text{bare}}_{K^*}$ as a function of time, on the 16^3 (top panel) and 24^3 (bottom panel) lattices. Symbols are the same as in Fig. 1.

$C_{V_iV_i}(t, \boldsymbol{p} = 0)$ over all three spatial directions. In the numerator, we average over $C_{\{41\}1}(t, \boldsymbol{p} = 0)$, $C_{\{42\}2}(t, \boldsymbol{p} = 0)$, and $C_{\{43\}3}(t, \boldsymbol{p} = 0)$. Results are shown in Fig. 2. $\langle\xi^2\rangle^{\|\text{bare}}_{K^*,\rho,\phi}$ is extracted from the ratio defined in (28b) by averaging $C_{V_iV_i}(t, p_i = 0, |\boldsymbol{p}| = \frac{2\pi}{L})$ over all four appropriate momenta for all three spatial directions in the denominator. In the numerator we average over all possible combinations of $C_{\{4ij\}i}(t, p_j = \pm\frac{2\pi}{L}, |\boldsymbol{p}| = \frac{2\pi}{L})$ with $i \neq j$. There are no disconnected contributions for the K and K^* correlation functions. The π and ρ are isospin triplets and therefore have no disconnected contributions in our isospin-conserving calculations (for the neutral π and ρ there is an explicit cancellation of disconnected diagrams with u and d quarks when the quarks have the same mass). In principle, we should include disconnected contributions for the ϕ. However, we argue that these contributions are Zweig suppressed and can be neglected. We are not aware of existing computations of these terms. It would be of great interest to evaluate them in future work, but this is a challenging computation.

If picking the fit range was not straightforward, we considered the correlation functions in the numerator and denominator separately. We identified and excluded from our fits the region where the excited states still contributed. We then chose the fit range, aiming for a good χ^2/d.o.f. and a stable fit with respect to small variations of the lower bound of the range. Owing to the increasing noise when t gets larger, the fits are insensitive to the upper bound of the fit range.

The 16^3 and 24^3 bare results are given in Tables IV and V, respectively, complete with linear chiral extrapolations which, as we shall discuss in the next section, can be justified using chiral perturbation theory (at least in the pseudoscalar case).

C. Quark-mass extrapolations

In leading-order SU(3) chiral perturbation theory [57], $\langle\xi^1\rangle_K$ is proportional to $m_s - m_{u/d}$ without chiral logarithms:

$$\langle\xi^1\rangle_K = \frac{8B_0}{f^2}(m_s - m_{u/d})b_{1,2}, \tag{32}$$

where f and B_0 denote the usual chiral perturbation theory parameters and $b_{1,2}$ is a Wilson coefficient introduced in [57]. Our data show clearly the effects of SU(3) symmetry breaking and are compatible with this expectation. However, our results are at fixed m_s and we wish to extrapolate in the light-quark mass m_q. Our collaboration's recent experience is that the physical strange-quark mass is rather large for low-order chiral perturbation theory and so we should perform SU(2) chiral fits in the light quarks at fixed (large) m_s. For the first moment this implies a fit

TABLE IV. Summary of results for the bare values of the distribution amplitude moments on the 16^3 lattices. The chiral extrapolations are discussed in Sec. III C, and the errors are statistical and (in the first-moment case) due to the uncertainty in the physical point for the chiral extrapolation.

am_{ud}	0.03	0.02	0.01	0.005	χ limit
$\langle\xi^2\rangle^{\text{bare}}_{\pi}$	0.110(2)	0.109(2)	0.113(4)	...	0.112(5)
$\langle\xi^1\rangle^{\text{bare}}_{K}$	0.005 43(27)	0.011 74(71)	0.0194(15)	...	0.0228(14)(11)
$\langle\xi^2\rangle^{\text{bare}}_{K}$	0.109(2)	0.107(2)	0.113(3)	...	0.112(4)
$\langle\xi^2\rangle^{\|\text{bare}}_{\rho}$	0.113(4)	0.100(5)	0.116(6)	...	0.109(10)
$\langle\xi^1\rangle^{\|\text{bare}}_{K^*}$	0.006 10(24)	0.012 75(51)	0.0207(10)	...	0.024 43(96)(107)
$\langle\xi^2\rangle^{\|\text{bare}}_{K^*}$	0.111(4)	0.101(4)	0.113(4)	...	0.110(6)
$\langle\xi^2\rangle^{\|\text{bare}}_{\phi}$	0.109(3)	0.100(3)	0.109(3)	...	0.107(5)

TABLE V. Summary of results for the bare values of the distribution amplitude moments on the 24^3 lattices.

am_{ud}	0.03	0.02	0.01	0.005	χ limit
$\langle\xi^2\rangle^{\text{bare}}_{\pi}$	0.103(9)	0.104(6)	0.114(3)	0.121(9)	0.125(7)
$\langle\xi^1\rangle^{\text{bare}}_{K}$	0.005 66(33)	0.012 54(72)	0.019 46(65)	0.0231(15)	0.023 77(71)(110)
$\langle\xi^2\rangle^{\text{bare}}_{K}$	0.103(8)	0.106(4)	0.112(2)	0.113(6)	0.117(5)
$\langle\xi^2\rangle^{\|\text{bare}}_{\rho}$	0.110(9)	0.093(10)	0.112(3)	0.120(13)	0.118(7)
$\langle\xi^1\rangle^{\|\text{bare}}_{K^*}$	0.006 19(35)	0.0139(10)	0.0225(13)	0.0311(30)	0.0281(13)(14)
$\langle\xi^2\rangle^{\|\text{bare}}_{K^*}$	0.109(12)	0.095(8)	0.108(3)	0.117(5)	0.118(7)
$\langle\xi^2\rangle^{\|\text{bare}}_{\phi}$	0.108(7)	0.097(7)	0.105(2)	0.107(3)	0.107(4)

function linear in the light-quark mass with coefficients depending on the strange-quark mass. The complete SU(2) chiral perturbation theory expression for the first moment must vanish when $m_q = m_s$ but this need not be so for the leading terms. We therefore perform a linear extrapolation in $a(m_s - m_q)$ to the physical point $a(m_s - m_{ud})$, without constraining the fit to vanish in the SU(3) limit, as shown in Fig. 3. The second error quoted in the results in the chiral limit for the first moments in Tables IV and V is due to the uncertainty in this physical point (determined using the quark masses in Table I). In this way we deal simultaneously with the usual light-quark-mass extrapolation and with the strange-quark-mass extrapolation which is necessitated by our strange-quark mass being approximately 15% too heavy.

A similar linear behavior is seen for $\langle \xi^1 \rangle^{\|\text{bare}}_{K^*}$ (see Fig. 3), so we follow the same extrapolation procedure. We note a hint of a finite volume effect in the K^* case but not in the K case, which is contrary to what we would expect. Where we have K^* results for both volumes at the same light-quark mass, however, they agree within the statistical uncertainties.

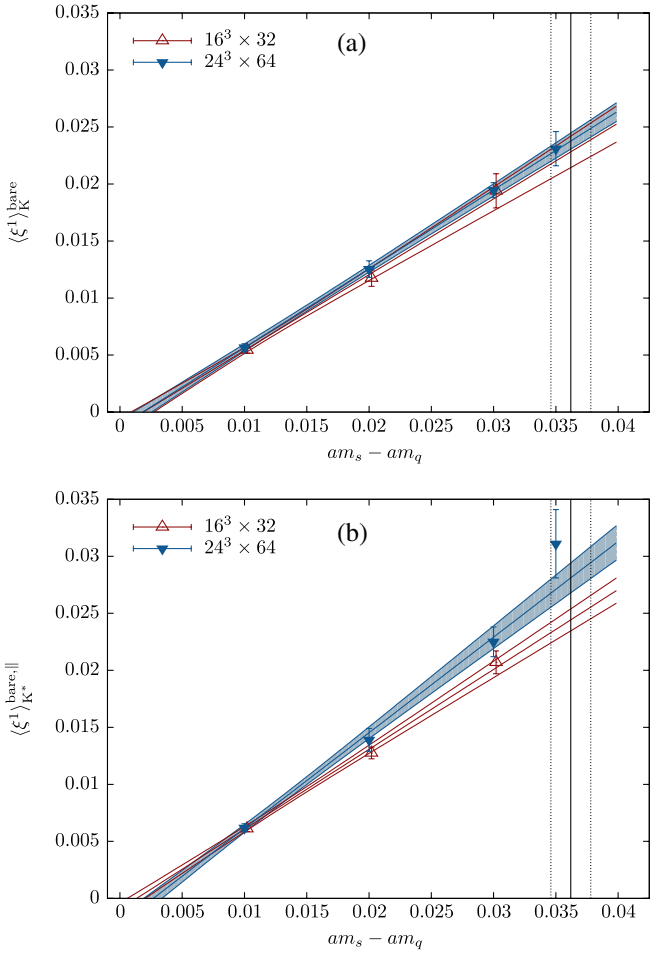

FIG. 3 (color online). Chiral extrapolations for $\langle \xi^1 \rangle^{\text{bare}}_K$ and $\langle \xi^1 \rangle^{\|\text{bare}}_{K^*}$. The extrapolation to the physical point is shown by the vertical solid line, with uncertainty, dominated by the uncertainty in the physical strange mass, indicated by the dotted lines.

For the second moments, we also have some guidance from chiral perturbation theory [58]; there is no nonanalytic dependence at one loop, and we should fit linearly in m_π^2. The dependence on the quark masses is very mild in any case, and in fact our results for the ρ, K^*, and ϕ agree within the statistical errors. Therefore, we perform a linear extrapolation in the light-quark masses and neglect the effect of the too-heavy strange-quark mass (see Fig. 4). We see no indication for finite size effects in the second moments when we compare the data points on the two different lattice volumes. They agree within their statistical errors.

IV. RENORMALIZATION OF THE LATTICE COMPOSITE OPERATORS

We now discuss the conversion of our bare lattice results to results in the $\overline{\text{MS}}$ scheme. To reduce systematic uncertainties we have determined the renormalization factors nonperturbatively in the modified regularization-independent momentum (RI′/MOM) scheme, continuing the work in [59], and we convert to $\overline{\text{MS}}$ using three-loop continuum perturbation theory [60,61]. We begin, however, with a perturbative calculation of the renormalization factors. The perturbative results have been used previously in [62,63] and will provide a comparison to the nonperturbative results. The contribution to the second moment from mixing with a total-derivative operator is calculated perturbatively only. We will see that this contribution is small and is not accessible within the current nonperturbative scheme.

A. Perturbative renormalization

The perturbative matching from the lattice to $\overline{\text{MS}}$ schemes is performed by comparing one-loop calculations of quark two-point one particle irreducible (1PI) functions with an insertion of the relevant bare lattice operator. This requires the evaluation of the diagrams shown in Fig. 5, together with wavefunction renormalization factors, Fig. 6. For the first-moment operator, we define

$$\mathcal{O}^{\overline{\text{MS}}}_{\{\rho\mu\}}(\mu) = Z_{\mathcal{O}_{\{\rho\mu\}}}(\mu a)\mathcal{O}^{\text{latt}}_{\{\rho\mu\}}(a). \tag{33}$$

For the second-moment calculation we must take account of mixing with a total-derivative operator (cf. Sec. II B). Adopting the notation

$$\begin{aligned} \mathcal{O}_{DD} &= \bar{\psi}\gamma_{\{\mu}\gamma_5 \overleftrightarrow{D}_\nu D_{\kappa\}} \overleftrightarrow{D}_\kappa \psi, \\ \mathcal{O}_{\partial\partial} &= \partial_{\{\nu}\partial_\kappa \bar{\psi}\gamma_{\mu\}}\gamma_5 \psi, \end{aligned} \tag{34}$$

with all Lorentz indices distinct and symmetrized, we need to determine

$$\mathcal{O}_{DD}^{\overline{\mathrm{MS}}}(\mu) = Z_{DD,DD}(\mu a)\mathcal{O}_{DD}^{\mathrm{latt}}(a) + Z_{DD,\partial\partial}(\mu a)\mathcal{O}_{\partial\partial}^{\mathrm{latt}}(a). \tag{35}$$

The renormalization factors are given by

$$Z_{\mathcal{O}_{\{\rho\mu\}}}(\mu a) = \frac{1}{(1-w_0^2)Z_w}\Big[1 + \frac{\alpha C_{\mathrm{F}}}{4\pi}\Big(-\frac{16}{3}\ln(\mu a) + \Sigma_1^{\overline{\mathrm{MS}}} - \Sigma_1 + V^{\overline{\mathrm{MS}}} - V\Big)\Big], \tag{36}$$

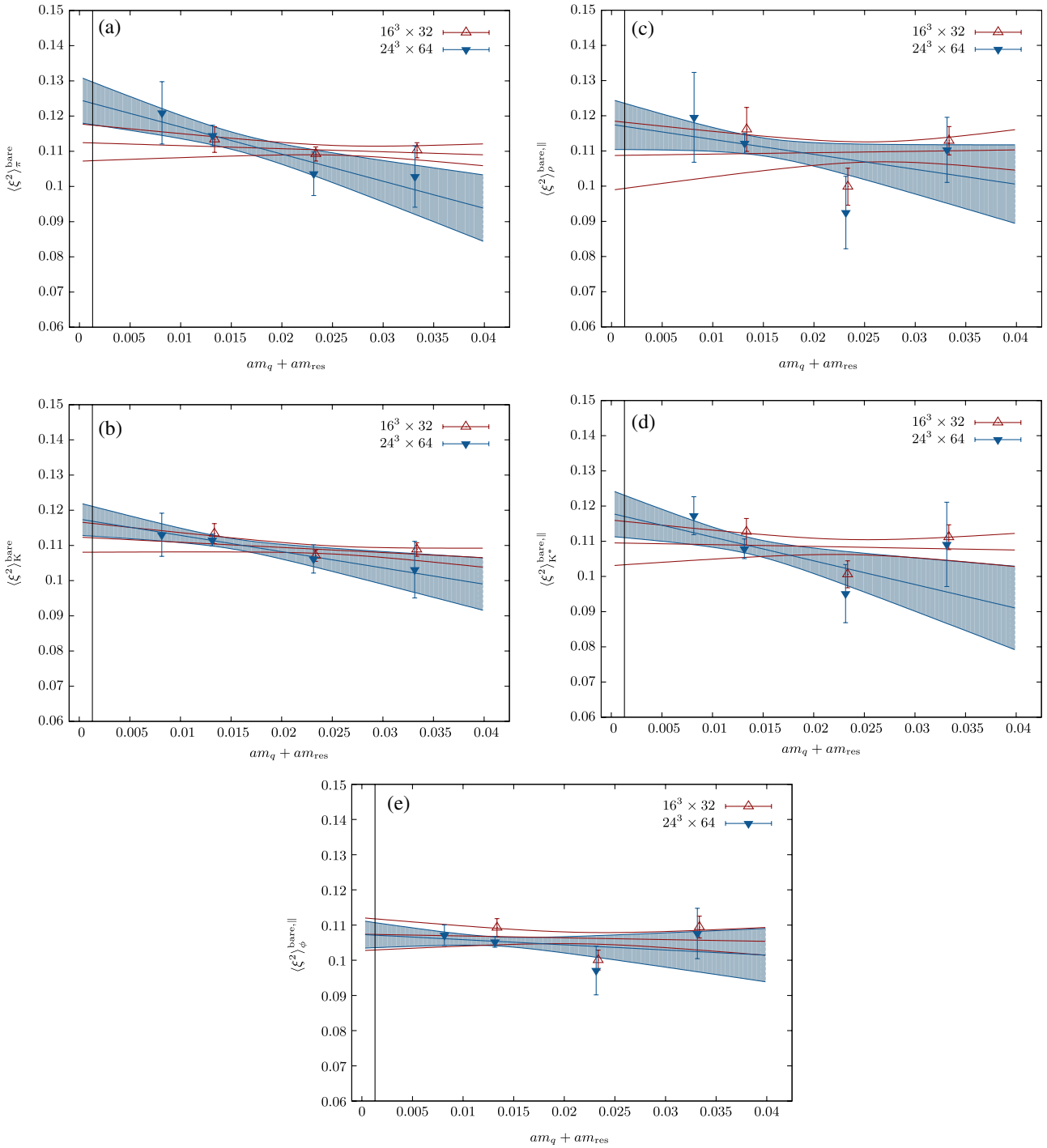

FIG. 4 (color online). Chiral extrapolations for $\langle \xi^2 \rangle_\pi^{\mathrm{bare}}$, $\langle \xi^2 \rangle_K^{\mathrm{bare}}$, $\langle \xi^2 \rangle_\rho^{\|\mathrm{bare}}$, $\langle \xi^2 \rangle_{K^*}^{\|\mathrm{bare}}$, and $\langle \xi^2 \rangle_\phi^{\|\mathrm{bare}}$. The physical value for $am_q + am_{\mathrm{res}}$ is shown by the solid vertical line in each case.

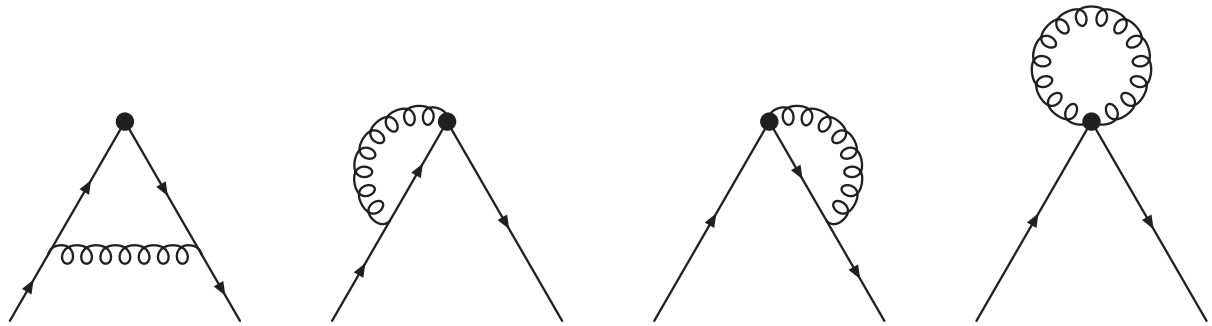

FIG. 5. One-loop vertex diagrams evaluated in the perturbative renormalization of the first- and second-moment operators.

$$Z_{DD,DD}(\mu a) = \frac{1}{(1-w_0^2)Z_w}\Big[1 + \frac{\alpha C_F}{4\pi}\Big(-\frac{25}{3}\ln(\mu a) + \Sigma_1^{\overline{\rm MS}} - \Sigma_1 + V_{DD}^{\overline{\rm MS}} - V_{DD}\Big)\Big], \tag{37}$$

$$Z_{DD,\partial\partial}(\mu a) = \frac{1}{(1-w_0^2)Z_w}\,\frac{\alpha C_F}{4\pi}\Big(\frac{5}{3}\ln(\mu a) + V_{\partial\partial}^{\overline{\rm MS}} - V_{\partial\partial}\Big). \tag{38}$$

In the equations above $(1-w_0^2)Z_w$ is a characteristic normalization factor for the physical quark fields in the domain-wall formalism. Z_w represents an additive renormalization of the large Dirac mass or domain-wall height $M = 1 - w_0$, which can be rewritten in multiplicative form at one loop as

$$Z_w = 1 + \frac{\alpha C_F}{4\pi} z_w, \qquad z_w = \frac{2w_0}{1-w_0^2}\Sigma_w. \tag{39}$$

The one-loop correction z_w becomes very large for certain choices of M [64,65], including that used in our numerical simulations, so that some form of mean-field improvement is necessary, as discussed below.

Terms with superscripts $\overline{\rm MS}$ in Eqs. (36)–(38) arise from the continuum calculations, while unsuperscripted terms come from the computations in the lattice scheme. To shorten some expressions, below we will define

$$c = \Sigma_1^{\overline{\rm MS}} - \Sigma_1 + V^{\overline{\rm MS}} - V, \tag{40}$$

$$c_{DD} = \Sigma_1^{\overline{\rm MS}} - \Sigma_1 + V_{DD}^{\overline{\rm MS}} - V_{DD}, \tag{41}$$

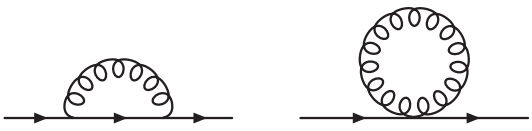

FIG. 6. One-loop diagrams for the quarks' wavefunction renormalization.

$$c_{\partial\partial} = V_{\partial\partial}^{\overline{\rm MS}} - V_{\partial\partial}. \tag{42}$$

The terms $\Sigma_1^{\overline{\rm MS}}$ and Σ_1 come from quark wavefunction renormalization, while $V^{\overline{\rm MS}}$, $V_{DD}^{\overline{\rm MS}}$, $V_{\partial\partial}^{\overline{\rm MS}}$ and V, V_{DD}, $V_{\partial\partial}$ come from the one-loop corrections to the amputated two-point function. They are given by "vertex" and "sail" diagrams, plus an operator tadpole diagram in the lattice case. $V_{DD}^{\overline{\rm MS}}$ and V_{DD} can be isolated by computing the one-loop correction with equal incoming and outgoing quark momenta. Likewise, $V_{\partial\partial}^{\overline{\rm MS}}$ and $V_{\partial\partial}$ are found by setting the incoming and outgoing quark momenta equal and opposite (the lattice tadpole diagram does not contribute in this case). Using naive dimensional regularization (NDR) in Feynman gauge with a gluon mass IR regulator,

$$\Sigma_1^{\overline{\rm MS}} = \frac{1}{2}, \qquad V^{\overline{\rm MS}} = -\frac{25}{18}, \tag{43}$$

$$V_{DD}^{\overline{\rm MS}} = -\frac{121}{72}, \qquad V_{\partial\partial}^{\overline{\rm MS}} = \frac{41}{72}. \tag{44}$$

The lattice contributions are evaluated for domain-wall fermions with the Iwasaki gluon action ($c_1 = -0.331$), also choosing Feynman gauge and using a gluon mass IR regulator. Σ_1 has been evaluated in [65], while we calculated the vertex term V for the first-moment operator in [41]. Here we have calculated the vertex terms V_{DD} and $V_{\partial\partial}$ for the second-moment operator. Perturbative calculations with domain-wall fermions are explained in [64,65], and the form of the Iwasaki gluon propagator can be found in [66]. Values for Σ_1, V, V_{DD}, and $V_{\partial\partial}$ are given as functions of M in Table VI, along with c, c_{DD}, and $c_{\partial\partial}$. Chiral symmetry of the domain-wall action implies that these results also apply for the operators which are like those used here, but without the γ_5. We note that the perturbative renormalization factor for the first-moment operator using alternative fermion and gauge formulations can be found in [67] (domain-wall fermions and plaquette action), [68] (overlap fermions and Lüscher–Weisz action), and [69] (clover fermions and plaquette action). Second-moment calculations with clover and Wilson fermions

TABLE VI. Constants needed for the perturbative renormalization of the first- and second-moment operators using domain-wall fermions and the Iwasaki gauge action ($c_1 = -0.331$). M is the domain-wall height, $c = \Sigma_1^{\overline{\rm MS}} - \Sigma_1 + V^{\overline{\rm MS}} - V$, $c_{DD} = \Sigma_1^{\overline{\rm MS}} - \Sigma_1 + V_{DD}^{\overline{\rm MS}} - V_{DD}$, and $c_{\partial\partial} = V_{\partial\partial}^{\overline{\rm MS}} - V_{\partial\partial}$. Σ_1, V, V_{DD}, and $V_{\partial\partial}$ are dependent on the gauge and the infrared regulator: Feynman gauge and a gluon mass are used here. V was calculated in [41], while V_{DD} and $V_{\partial\partial}$ have been calculated as part of this work.

M	Σ_1	V	c	V_{DD}	c_{DD}	$V_{\partial\partial}$	$c_{\partial\partial}$
0.1	4.6519	−4.6297	−0.9110	−10.816	4.9838	0.5415	0.0279
0.2	4.5193	−4.5614	−0.8468	−10.698	4.9982	0.4285	0.1409
0.3	4.4093	−4.5101	−0.7881	−10.608	5.0179	0.3433	0.2262
0.4	4.3158	−4.4678	−0.7369	−10.533	5.0362	0.2729	0.2966
0.5	4.2354	−4.4311	−0.6932	−10.467	5.0509	0.2119	0.3575
0.6	4.1665	−4.3980	−0.6574	−10.407	5.0603	0.1573	0.4122
0.7	4.1079	−4.3673	−0.6295	−10.352	5.0639	0.1070	0.4625
0.8	4.0593	−4.3381	−0.6101	−10.300	5.0604	0.0597	0.5098
0.9	4.0204	−4.3097	−0.5996	−10.250	5.0489	0.0142	0.5552
1.	3.9915	−4.2816	−0.5988	−10.200	5.0283	−0.0303	0.5998
1.1	3.9731	−4.2529	−0.6090	−10.151	4.9970	−0.0749	0.6443
1.2	3.9664	−4.2232	−0.6321	−10.100	4.9528	−0.1205	0.6899
1.3	3.9727	−4.1916	−0.6700	−10.047	4.8933	−0.1682	0.7376
1.4	3.9943	−4.1571	−0.7261	−9.9895	4.8147	−0.2195	0.7889
1.5	4.0343	−4.1182	−0.8050	−9.9267	4.7119	−0.2764	0.8458
1.6	4.0974	−4.0728	−0.9135	−9.8551	4.5771	−0.3418	0.9112
1.7	4.1905	−4.0176	−1.0618	−9.7700	4.3989	−0.4205	0.9899
1.8	4.3249	−3.9462	−1.2676	−9.6627	4.1572	−0.5211	1.0905
1.9	4.5209	−3.8447	−1.5651	−9.5140	3.8125	−0.6631	1.2325

have been performed in [69,70], respectively (in both cases using the plaquette action).

Our numerical simulations use $M = 1.8$. For this value of M, with the Iwasaki gluon action, the one-loop coefficient in the physical quark normalization is $z_w \approx 112$ (extracted from Σ_w in Table III of [65]), making it clear that mean-field improvement is necessary. We follow the prescription given in [65]. The first step is to define a mean-field value for the domain-wall height,

$$M^{\rm MF} = M - 4(1 - P^{1/4}) = 1.3029, \tag{45}$$

where $P = 0.588\,13(4)$ is the average plaquette value in the chiral limit in our simulations. The physical quark normalization factor becomes $[1 - (w_0^{\rm MF})^2]Z_w^{\rm MF}$, with

$$\begin{aligned} Z_w^{\rm MF} &= 1 + \frac{\alpha C_{\rm F}}{4\pi} z_w^{\rm MF}, \\ z_w^{\rm MF} &= \frac{2w_0^{\rm MF}}{1 - (w_0^{\rm MF})^2}(\Sigma_w + 32\pi^2 T_{\rm MF}) = 5.2509, \end{aligned} \tag{46}$$

where $T_{\rm MF} = 0.052\,566\,4$ [65] is a mean-field tadpole factor and Σ_w is evaluated at $M^{\rm MF}$. Values for $z_w^{\rm MF}$ as a function of M are quoted in Table VII, extracted from the results in [65]. Likewise, $\Sigma_1 = 3.9731$, $V = -4.1907$, $V_{DD} = -10.045$, and $V_{\partial\partial} = -0.1696$ are evaluated at $M^{\rm MF}$.

TABLE VII. Values for z_w, $z_w^{\rm MF}$ extracted from the results in [65], and d_f extracted from [71].

M	z_w	$z_w^{\rm MF}$	d_f
0.1	−243.86	−86.579	−0.023 03
0.2	−113.29	−39.501	−0.017 98
0.3	−69.404	−23.830	−0.014 97
0.4	−47.077	−15.949	−0.012 74
0.5	−33.278	−11.142	−0.010 90
0.6	−23.648	−7.8365	−0.009 315
0.7	−16.300	−5.3538	−0.007 896
0.8	−10.263	−3.3459	−0.006 589
0.9	−4.9617	−1.6078	−0.005 379
1.0	0.0	0.0	−0.004 261
1.1	4.9442	1.5902	−0.003 227
1.2	10.192	3.2748	−0.002 290
1.3	16.136	5.1900	−0.001 485
1.4	23.346	7.5350	−0.000 865 0
1.5	32.784	10.648	−0.000 536 0
1.6	46.322	15.194	−0.000 656 6
1.7	68.294	22.720	−0.001 570
1.8	111.69	37.901	−0.004 014
1.9	241.55	84.270	−0.010 20

For the operator $\mathcal{O}_{DD}$ with two covariant derivatives, mean-field improvement introduces a factor $u_{\rm pt}/u$, where u is the mean link (here taken to be $u = P^{1/4}$) and

$$u_{\rm pt} = 1 - \frac{\alpha C_{\rm F}}{4\pi} 8\pi^2 T_{\rm MF}$$

is its perturbative expansion. For $\mathcal{O}_{\partial\partial}$ with two ordinary derivatives, in contrast, the extra factor is $u/u_{\rm pt}$. The mean-field-improved matching factors are thus

$$Z^{\rm MF}_{\mathcal{O}_{\{\rho\mu\}}} = \frac{1}{1-(w_0^{\rm MF})^2}\frac{1}{Z_w^{\rm MF}}\left[1+\frac{\alpha C_{\rm F}}{4\pi}\left(-\frac{16}{3}\ln(\mu a)+c^{\rm MF}\right)\right], \tag{47}$$

$$Z^{\rm MF}_{DD,DD} = \frac{1}{u}\frac{1}{1-(w_0^{\rm MF})^2}\frac{1}{Z_w^{\rm MF}}\left[1+\frac{\alpha C_{\rm F}}{4\pi}\left(-\frac{25}{3}\ln(\mu a) + c^{\rm MF}_{DD} - 8\pi^2 T_{\rm MF}\right)\right], \tag{48}$$

$$Z^{\rm MF}_{DD,\partial\partial} = u\frac{1}{1-(w_0^{\rm MF})^2}\frac{1}{Z_w^{\rm MF}}\frac{\alpha C_{\rm F}}{4\pi}\left(\frac{5}{3}\ln(\mu a)+c^{\rm MF}_{\partial\partial}\right), \tag{49}$$

with $c^{\rm MF} = -0.6713$, $c^{\rm MF}_{DD} - 8\pi^2 T_{\rm MF} = 0.7408$, and $c^{\rm MF}_{\partial\partial} = 0.7391$. To evaluate these expressions, we make two choices for the coupling. The first is a mean-field improved coupling defined using the measured plaquette value P, according to [71]

$$\frac{1}{g^2_{\rm MF}(\mu)} = \frac{P}{g_0^2} + d_g + c_p + \frac{22}{16\pi^2}\ln(\mu a) + N_f\left[d_f - \frac{4}{48\pi^2}\ln(\mu a)\right], \tag{50}$$

where N_f is the number of dynamical quark flavors. For the Iwasaki gauge action with $c_1 = -0.331$, the values $d_g = 0.1053$ and $c_p = 0.1401$ are given in [65], while values for d_f as a function of M were calculated in [71] and are quoted in Table VII. In our simulations, $\beta = 6/g_0^2 = 2.13$ with $N_f = 3$ and $a^{-1} = 1.729$ GeV. The second choice is the continuum $\overline{\rm MS}$ coupling, calculated as outlined in Appendix A of [59]. At $\mu a = 1$, we find $\alpha_{\rm MF} = 0.1769$ and $\alpha^{\overline{\rm MS}} = 0.3138$. We use these two values to evaluate the renormalization factors above. We also evaluate the mean-field improved expression for the axial-vector current renormalization [65], interpolating to our mean-field $M^{\rm MF}$. The values are shown in Table VIII. The ratios of the renormalization factors, from which the factor $1/(1-(w_0^{\rm MF})^2)Z_w^{\rm MF}$ cancels, are also shown in the table.

We take the mean value of the results with the two different choices for the coupling as the best answer for the renormalization factors. The difference between the two choices will form the error. The relevant factors for the perturbative renormalization of the ratios in Eqs. (25) and (28) are given in Table IX. Chiral symmetry here ensures that we do not have to distinguish between vector and axial-vector operators. We note that the contribution from the mixing term $Z_{DD,\partial\partial}$ is smaller than the error on $Z_{DD,DD}$ itself.

TABLE VIII. Perturbative renormalization factors and their ratios for two choices of the strong coupling, evaluated at $\mu a = 1$.

	$Z^{\rm MF}_{\mathcal{O}_{\{\rho\mu\}}}$	$Z^{\rm MF}_{DD,DD}$	$Z^{\rm MF}_{DD,\partial\partial}$	$Z^{\rm MF}_{\rm A}$	$\frac{Z^{\rm MF}_{\mathcal{O}_{\{\rho\mu\}}}}{Z^{\rm MF}_{\rm A}}$	$\frac{Z^{\rm MF}_{DD,DD}}{Z^{\rm MF}_{\rm A}}$	$\frac{Z^{\rm MF}_{DD,\partial\partial}}{Z^{\rm MF}_{\rm A}}$
$\alpha_{\rm MF}$	0.9896	1.1604	0.0122	0.8009	1.2356	1.4488	0.0152
$\alpha^{\overline{\rm MS}}$	0.9162	1.0966	0.0202	0.6934	1.3214	1.5815	0.0291

TABLE IX. Perturbative renormalization factors to match the lattice results to $\overline{\rm MS}$ at $a\mu = 1$.

$\frac{Z_{\mathcal{O}_{\{\rho\mu\}}}}{Z_{\rm A}}$	$\frac{Z_{DD,DD}}{Z_{\rm A}}$	$\frac{Z_{DD,\partial\partial}}{Z_{\rm A}}$
1.28(4)	1.52(7)	0.022(7)

B. Nonperturbative renormalization

In order to renormalize the correlation functions nonperturbatively we make use of the Rome-Southampton RI′/MOM scheme [72], which we now briefly review and discuss refinements to [59]. The starting point and definition of the RI′/MOM scheme is a simple renormalization condition that can be imposed independently of the regularization used, thus on the lattice as well as in the continuum. This facilitates scheme changes, which is important for the matching to $\overline{\rm MS}$. The renormalization condition has the form

$$\Lambda_{\mathcal{O}}(p) = Z_{\mathcal{O}}(\mu)Z_q^{-1}(\mu)\Lambda^{\rm bare}_{\mathcal{O}}(p)|_{p^2=\mu^2} = \Lambda^{\rm tree}_{\mathcal{O}}(p), \tag{51}$$

where $\Lambda_{\mathcal{O}}$ ($\Lambda^{\rm bare}_{\mathcal{O}}$) is the renormalized (bare) vertex amplitude. Together with the quark field renormalization $Z_q^{1/2}$, defined by $\psi = Z_q^{1/2}\psi^{\rm bare}$, this defines the renormalization constant $Z_{\mathcal{O}}$ for the operator $\mathcal{O}$. The renormalization scale μ is set by the momentum of the external states entering the vertex amplitude. In the original RI′/MOM scheme these momenta are *exceptional*, that is, equal incoming and outgoing quark momenta, p and p'. For some renormalization factors it is advantageous to use a nonexceptional symmetric choice of momenta $p^2 = p'^2 = q^2$, where $q = p - p'$, leading to the distinct regularization-independent momentum scheme with a symmetric choice of momenta. This suppresses unwanted infrared effects in the vertex amplitude, pion poles for example, and suggests a better-behaved accompanying continuum perturbation theory [73]. Exceptional momenta with $q = 0$ also cause matrix elements of operators with total derivatives to vanish, making $Z_{DD,\partial\partial}$ inaccessible in our nonperturbative analysis.

The vertex amplitude is constructed from the unamputated Green's function

$$G_{\mathcal{O}}(p) = \langle\psi(p)\mathcal{O}(0)\bar\psi(p)\rangle, \qquad \mathcal{O}(0) = \sum_{x,x'}\bar\psi(x)J_{\mathcal{O}}(x,x')\psi(x'). \tag{52}$$

The external quark lines need gauge fixing, for which we use Landau gauge. The current J has the appropriate Dirac structure and may be nonlocal if the operator contains derivatives. For example, a single right derivative $\vec{D}_\nu$ in the vector case would correspond to

$$J_{\mathcal{O}_{\rho\mu}}(x,x') = \gamma_\rho \tfrac{1}{2}(U(x,x')\delta_{x',x+\hat{\mu}} - U(x,x')\delta_{x',x-\hat{\mu}}) \quad (53)$$

matching the definition in Eq. (18).

The vertex amplitude itself is found after amputating the Green's function and tracing with a suitable projector $P_{\mathcal{O}}$,

$$\Lambda_{\mathcal{O}}(p) = \mathrm{Tr}[\Pi_{\mathcal{O}}(p) P_{\mathcal{O}}], \quad (54)$$

$$\Pi_{\mathcal{O}}(p) = \langle S(p)\rangle^{-1} \langle G_{\mathcal{O}}(p)\rangle \langle S(p)\rangle^{-1}. \quad (55)$$

We have used the quark propagator $S(p)$, and the angle brackets indicate the gauge average. The projector $P_{\mathcal{O}}$ depends on the particular operator and includes an overall normalization factor to account for the color and Dirac trace. In a simple example $P_{\mathcal{O}}$ would isolate the tree-level contribution to the vertex amplitude; we will detail our choices below. We have now defined the renormalization procedure and will turn to details of the implementation before discussing the results.

1. Momentum sources

One refinement to our previous work [59] is the use of momentum sources [74]. In contrast to the point sources used before, this effectively amounts to a volume average over the lattice, resulting in much smaller statistical errors [63]. Starting from (52) the Green's function in momentum space is

$$G_{\mathcal{O}}(p) = \sum_{x,x'} \langle \gamma_5 S^\dagger(p)_x \gamma_5 J_{\mathcal{O}}(x,x') S(p)_{x'} \rangle, \quad (56)$$

where rather than using the quark propagator $S(x|y)$ obtained by inverting the Dirac matrix M on a point source

$$\sum_x M(x',x) S(x|y) = \delta_{x',y}, \quad (57)$$

we use $S(p)_x = \sum_y S(x|y) e^{ipy}$, which can be found by inverting with a momentum source [74]

$$\sum_x M(x',x) S(p)_x = e^{ipx'}, \quad (58)$$

and is defined on all lattice sites corresponding to the off-shell quarks used in the Green's function. The gain in statistical accuracy is paid for with a separate inversion for every momentum used in the simulation. However, this is more than compensated by a much reduced number of necessary configurations. Limiting ourselves to a few carefully chosen momenta, statistical fluctuations are reduced with lower overall computational cost.

The momenta we use are, first of all, constrained to be within a range $\Lambda_{\mathrm{QCD}} \ll p^2 \ll 1/a$ for the RI′/MOM scheme [72]. We use our previous results [59] to identify suitable values and focus on momenta which are expected to have reduced hypercubic lattice artefacts by trying to limit $\sum p_\mu^4$ for fixed p^2 [63] (see also [75,76]). The values used are

$16^3 \times 32$: (1,1,2,3), (1,1,2,4), (1,2,2,1), (1,2,2,3), (1,2,2,4)

and

$24^3 \times 64$: (2,2,2,7), (2,2,2,8), (2,2,3,7), (2,2,3,8), (2,3,3,7),

where we have given n_μ^T for momenta $p_\mu = 2\pi n_\mu / L$ (with $L \to T$ for time components).

2. Projectors

We extend the set of operators considered previously in [59]. We now require operators with up to two derivatives, $\mathcal{O}^{(5)}_{\{\mu_1 \ldots \mu_n\}}$ $(n \le 3)$, making the necessary projectors $P_{\mathcal{O}}$ slightly more involved than for bilinears. Since we resort to readily available calculations [60,61,77] for the final conversion to $\overline{\mathrm{MS}}$, as well as to account for running, we have to tailor the projectors to match the RI′/MOM scheme and vertex functions used in the continuum calculations. Decomposing the amputated Green's function into terms allowed by Lorentz symmetry and remembering that we are taking all indices to be distinct, we find [60,61,77]

$$G_{\mathcal{O}}(p) = \Sigma_1(p) \gamma_{\{\mu_1} p_{\mu_2} \ldots p_{\mu_n\}} + \Sigma_2(p) p_{\mu_1} \ldots p_{\mu_n} \not{p}. \quad (59)$$

For simplicity, we limit the discussion to the vector case here; axial-vector operators are analogous. The RI′/MOM scheme uses the contribution from $\Sigma_1(p)$ only in (59). The required projector $P_{\mathcal{O}}$ will depend on the momentum entering the Green's function and its (fixed) directions μ_i $(i = 1 \ldots n)$. In general, multiplying $G_{\mathcal{O}}$ with γ_{μ_i} picks up combinations of both terms Σ_1 and Σ_2. On the other hand, projecting with γ_ρ, where $\rho \notin \{\mu_i\}$, is sensitive only to Σ_2 (note that we have $n \le 3$). Thus multiplying with the difference of the two Dirac matrices with appropriate normalization and momentum factors ensures that the vertex amplitude in (54) contains $\Sigma_1(p)$ only. There are simpler special cases in which one or more components of the momentum p are zero, causing the second term in (59) to vanish. However, since we tried to choose our momentum directions close to the diagonal of the lattice, we do not have momentum components that are zero.

For fixed indices μ_i $(i = 1 \ldots n)$ of the Green's function, we can construct n different projectors $P_{\mathcal{O},i}$ by starting from any of the γ_{μ_i}:

$$P_{\mathcal{O},i} = \frac{\gamma_{\mu_i} - \gamma_\rho \frac{\bar{p}_{\mu_i}}{\bar{p}_\rho}}{\mathcal{N} \prod_{j \ne i, j=1}^n \bar{p}_{\mu_j}}, \quad \text{with} \quad i = 1 \ldots n. \quad (60)$$

The normalization $\mathcal{N}$ is chosen such that for the tree-level vertex amplitude we find $\Lambda^{\mathrm{tree}}_{\mathcal{O}}(p) = 1$. The index ρ is different from any of the μ_i, such that its momentum component $\bar{p}_\rho$ is as small as possible to reduce discretization errors. We use $\bar{p}_\mu = \sin p_\mu$ to better account for lattice momenta. The case of axial-vector operators $\mathcal{O}^5$ is straightforward, with γ_5 inserted in the appropriate places.

Combining the n different $P_{\mathcal{O},i}$ with the possible index combinations of the Green's functions results in a total of 4, 12, and 12 ($n = 1, 2, 3$) choices to compute the vertex amplitude $\Lambda_{\mathcal{O}}(p)$ in Eq. (54), all of which should provide the same result for the final renormalization constant in the absence of lattice artefacts. Because of the different sized momentum components in different lattice directions, the expected discretization errors vary depending on the directions selected by the indices of the projector. These artefacts arise from breaking continuum O(4) symmetry to lattice hypercubic symmetry and are accounted for in the systematic error of our final results. With additional lattice spacings and the use of partially twisted boundary conditions, we could eliminate hypercubic lattice artefacts in the continuum limit [78,79].

3. Quark field renormalization

In general, the renormalization condition Eq. (51) requires knowledge of the field renormalization Z_q to obtain $Z_{\mathcal{O}}$. However, in the present calculation only ratios of renormalization factors of operators with one, two, or no derivatives appear, Eqs. (25) and (28). Combining this with our renormalization condition leads to

$$\frac{Z_{\mathcal{O},n=2,3}(\mu)}{Z_{\mathcal{O},n=1}(\mu)} = \frac{\Lambda^{\text{bare}}_{\mathcal{O},n=1}(p)}{\Lambda^{\text{bare}}_{\mathcal{O},n=2,3}(p)}\bigg|_{p^2=\mu^2}, \tag{61}$$

where the explicit Z_q dependence drops out. As mentioned earlier, we can use either the vector or axial-vector bilinears in this ratio thanks to chiral symmetry. We follow our earlier procedure [59] and average Λ_{γ_ρ} and $\Lambda^{(5)}_{\gamma_\rho}$ (Λ_V/Λ_A in the reference) to obtain our best answer. The analysis is also performed using $\Lambda^{(5)}_{\gamma_\rho}$ only, and the difference between the two results enters our systematic error.

4. Results for renormalization factors

Compared to [59] the reduced statistical errors make previously hidden systematic effects apparent and quantifiable [63] and affect the way we extract the renormalization factors. We start by considering different projectors for a fixed momentum p_μ of the external quarks; see Fig. 7. The results should be independent of the rotation and size of the momentum components used for the projector. The smaller statistical errors now reveal a disagreement due to lattice artefacts. We combine all choices for our best answer and account for the spread in our systematic error, improving previous estimates. Our general recipe to obtain the renormalization factors follows. The ratio of bare vertex amplitudes is extrapolated linearly to the chiral limit $m_q \to -m_{\text{res}}$ for each momentum. Only in the chiral limit can we remove the running of our data points and match them to a continuum scheme. So by using [60,61,77] we take our results from the RI′/MOM scheme at the scale

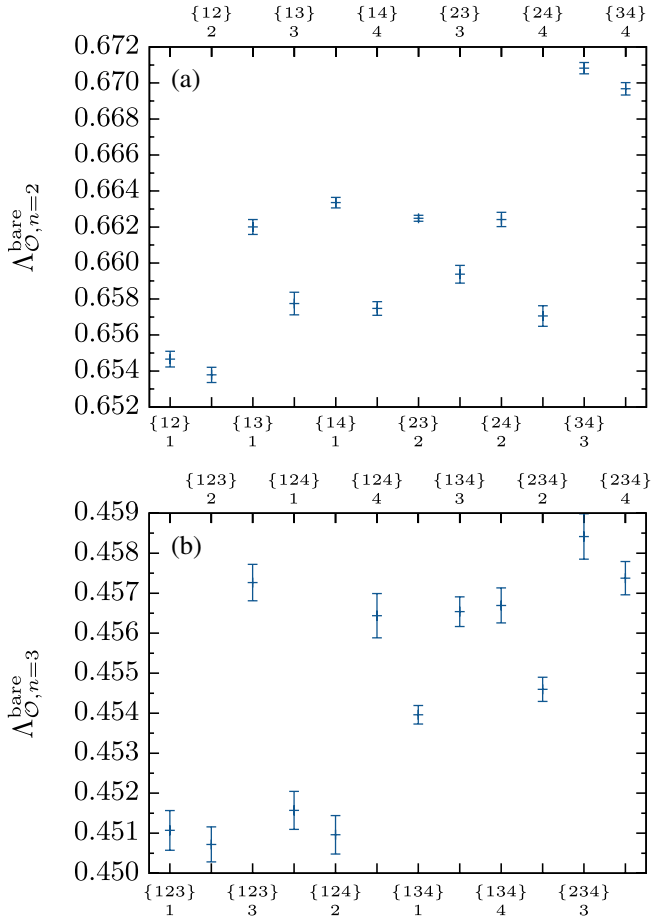

FIG. 7 (color online). Results for $\Lambda^{\text{bare}}_{\mathcal{O},n=2}$ ($\Lambda^{\text{bare}}_{\mathcal{O},n=3}$) are shown on the top (bottom) panel for a fixed momentum $(ap)^2 = 1.782\,01$, $p^T = (2, 2, 3, 8)$. The labels above and below the plots show the indices of the Green's function in brackets, $\{\mu_i\}$, with the index of the projector below. The disagreement between the different projections is due to lattice artefacts.

$\mu^2 = p^2$ to a common scale $\mu^2 = 4$ GeV^2 and convert to $\overline{\text{MS}}$ at that scale. The values thus obtained are then linearly interpolated to $p^2 = (2\text{ GeV})^2$ within our momentum window to obtain $Z_{\mathcal{O},n=2,3}/Z_{\mathcal{O},n=1}$ at a scale $\mu = 2$ GeV.

The central value is computed from the averaged values from all projectors and index combinations. A standard bootstrap analysis provides the statistical error which is inflated with $\sqrt{\chi^2/\text{d.o.f.}}$ (the PDG scale factor [80]) from the interpolation. Several effects are taken into account for the systematic error. Lattice artefacts are the dominant effect. To estimate those, we perform the analysis for all projectors separately as indicated above, and we choose the highest and lowest results for each momentum for the interpolation. From the two fits, the larger deviation from the central value then constitutes the systematic error from discretization effects (labeled ''spread'' in the final table). This is a conservative approach for the discretization error. Taking random choices of projectors (or, rather, their direction) for each momentum and looking at the 1σ width

of the range of results for many of those picks would lead to a smaller error. We account for missing higher-order terms in the continuum perturbative calculation via the slope of the momentum interpolation, using the difference of our results at $p^2 = (2\ \mathrm{GeV})^2$ and $(0\ \mathrm{GeV})^2$, indicated by "slope," as a measure. We note, however, that we cannot disentangle perturbative and discretization errors here and thus double count some of the discretization effects. Another source of systematic error is the strange-quark mass, kept fixed at $m_s = 0.04$ in our simulation. We deal with that as described at the end of Sec. IV.F in [59], estimating an error from half the linear dependence (slope) multiplied by the strange-quark mass m_s. This error is labeled "Δm_s." The last contribution to the systematic error is from the chiral symmetry breaking evident when comparing our vector and axial-vector operators [59,73,81]. This is estimated by the difference of the final results when taking the axial-vector bilinear ($n = 1$) or the averaged vector and axial-vector bilinear for the ratio in Eq. (61) (labeled "V-A"). Adding the four contributions in quadrature gives our systematic error.

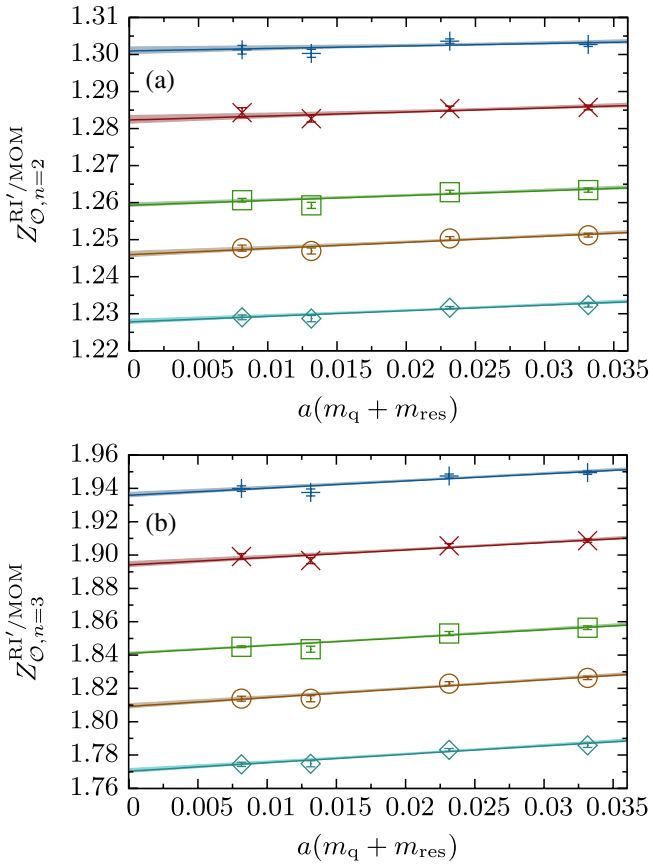

FIG. 8 (color online). Linear extrapolations of the renormalization factors to the chiral limit. The top panel shows $Z^{\mathrm{RI}'/\mathrm{MOM}}_{\mathcal{O},n=2}$, and the bottom plot is for $Z^{\mathrm{RI}'/\mathrm{MOM}}_{\mathcal{O},n=3}$. The momenta are increasing from top to bottom, and we have $(ap)^2 = 1.2947$, 1.4392, 1.6374, 1.7820, and 1.9801.

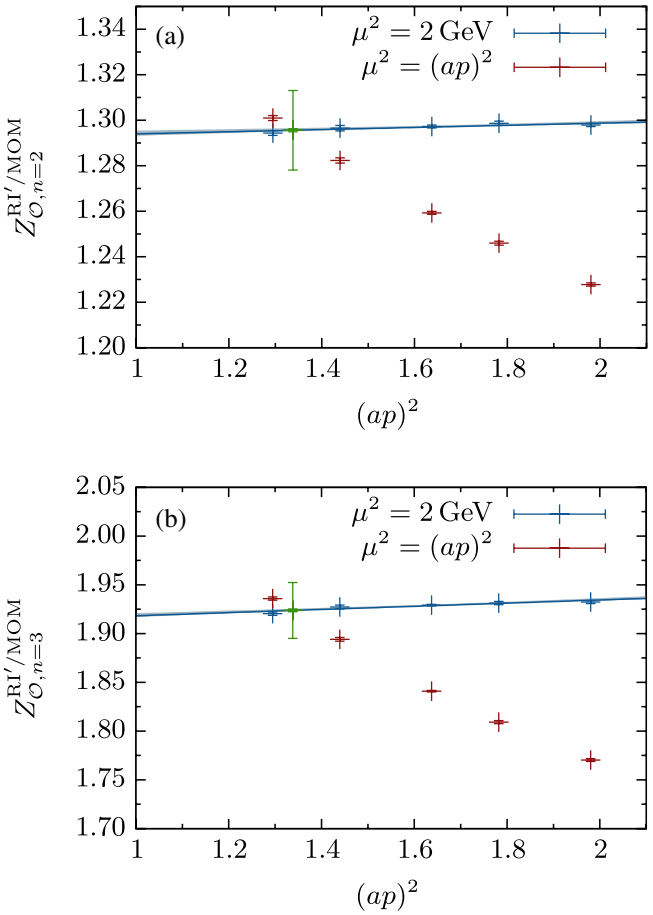

FIG. 9 (color online). These plots show both the scale-dependent Z's and the Z's for a fixed scale $\mu = 2$ GeV with the running successfully removed (both in RI′/MOM). The top (bottom) plot is for the one (two) derivative case. Also included is the linear interpolation to the final result, with the statistical error indicated by the error band. Our result at $\mu = 2$ GeV is then shown with error bars for the statistical and systematic errors.

To illustrate some of the steps mentioned above, we include in Fig. 8 two examples of the extrapolation to the chiral limit. Shown are extrapolations for all of our five momenta, for the renormalization factors for one and two derivatives. In Fig. 9 we show the renormalization factors before and after we remove the running, again for one and two derivatives. Once at a common scale, the data points are much flatter, indicating the validity of the scale conversion and the momentum window. Also included is the linear fit and our final result.

Our final values for the ratios of renormalization factors are given in Table X. These have been obtained using vectorlike operators. Results from the axial-vector operators are almost identical and show no low energy effects from breaking chiral symmetry, as for bilinears. We note that the renormalization factors are significantly different from 1 and deviate substantially from the perturbative results. Thus nonperturbative renormalization looks imperative here.

TABLE X. Final results for the renormalization factors in $\overline{\text{MS}}$ at $\mu = 2$ GeV. Results are given for both lattice sizes with all systematic errors. The perturbative results are also shown for comparison.

	$Z_{\mathcal{O}_{\{\rho\nu\}}}/Z_A$		$Z_{DD,DD}/Z_A$	
	$16^3 \times 32$	$24^3 \times 64$	$16^3 \times 32$	$24^3 \times 64$
Central value	1.545 75	1.528 93	2.060 64	2.028 00
Statistical error	0.002 49	0.000 81	0.004 82	0.001 49
Spread	0.029 68	0.018 09	0.037 02	0.015 34
Slope	0.004 70	0.007 43	0.000 97	0.022 85
Δm_s	0.000 89	0.002 32	0.004 69	0.009 92
V-A	0.007 23	0.006 02	0.009 38	0.007 60
Total error	0.031 02	0.020 61	0.038 79	0.030 26
Best result		1.5289(8)(206)		2.028(1)(30)
Perturbative result		1.24(3)		1.45(5)

C. Renormalized results

We now use the renormalization factors from the previous section to convert our bare lattice results to $\overline{\text{MS}}$ at $\mu = 2$ GeV. The local matrix elements in Eq. (9) require the renormalization factors $Z_{\mathcal{O}_{\{\rho\mu\}}}$, $Z_{DD,DD}$, and $Z_{DD,\partial\partial}$ as defined in Eqs. (33) and (35). The first two are computed nonperturbatively, while for the last one we use the perturbative result. From Eq. (35) we see that the mixing term requires the computation of a matrix element with an operator insertion of $\mathcal{O}_{\partial\partial}$. This is simplified since we use the ratios (25) and (28) to extract the moments of the distribution amplitudes. Within the ratios, the matrix element with the operator $\mathcal{O}_{\partial\partial}$ differs from the denominator only by the momentum factors and thus does not have to be computed separately. It contributes a constant shift to the result. To summarize,

$$\langle \xi^1 \rangle^{\overline{\text{MS}}} = \frac{Z_{\mathcal{O}_{\{\rho\mu\}}}}{Z_A} \langle \xi^1 \rangle^{\text{bare}}, \tag{62a}$$

$$\langle \xi^2 \rangle^{\overline{\text{MS}}} = \frac{Z_{DD,DD}}{Z_A} \langle \xi^2 \rangle^{\text{bare}} + \frac{Z_{DD,\partial\partial}}{Z_A}. \tag{62b}$$

With our best nonperturbative results from Table X and the perturbative result for the mixing term from Table IX [computed at the same scale of $\mu = 2$ GeV, $\frac{Z_{DD,\partial\partial}}{Z_A} = 0.027(8)$], we arrive at the renormalized moments of the distribution amplitudes given in Table XI. The contribution from the mixing term in Eq. (62b) is small, so using the perturbative result for $Z_{DD,\partial\partial}$ is not a drawback. Even if the correction of a nonperturbative result for $Z_{DD,\partial\partial}$ is as sizable as for $Z_{\mathcal{O}_{\{\rho\mu\}}}$ or $Z_{DD,DD}$, the overall contribution remains comparable to our present error on $Z_{DD,DD}/Z_A$. Hence our results are essentially renormalized nonperturbatively.

V. SUMMARY

We have computed the first or first two lowest nonvanishing moments of the distribution amplitudes of the π, K, K^*, ρ, and ϕ mesons, using nonperturbative renormalization of the lattice operators, with final numbers given in Table XI. Apart from the uncertainty in m_s for the first moments, systematic errors mainly come from the renormalization procedure. Within the current statistical errors on our data we do not see any finite size effects. With only one lattice spacing we can also only estimate a formal discretization error of $O(a^2\Lambda^2_{\text{QCD}}) \approx 4\%$ from the $O(a)$-improved DWF action and operators; this is included in our systematic error. The result for $\langle \xi^1 \rangle_K$ in Table XI supersedes but is compatible with our earlier result in [41,42], which was obtained on the $16^3 \times 32$ ensembles only and used perturbative renormalization.

Converting the lowest moment of the kaon distribution amplitude to the first Gegenbauer moment $a^1_K = 0.061(2)(4)$, we find it in agreement with sum rule results from Eq. (16) but with a much reduced uncertainty. We compare our results to those from the QCDSF Collaboration [23] in Table XII (preliminary results for the first moment of the vector meson distribution amplitudes are also available from QCDSF [27]). The results for $\langle \xi^1 \rangle_K$ differ significantly. However, we observe that our measurements correspond to pion masses in the range 330–670 MeV and are for $2 + 1$ dynamical flavors, whereas the QCDSF results are for pion masses around

TABLE XI. Final results in the chiral limit in $\overline{\text{MS}}$ at $\mu = 2$ GeV for both of our lattice volumes. The first error is statistical, and the second includes systematic errors from m_s, discretization, and renormalization.

	$\langle \xi^2 \rangle_\pi$	$\langle \xi^1 \rangle_K$	$\langle \xi^2 \rangle_K$	$\langle \xi^2 \rangle^{\parallel}_\rho$	$\langle \xi^1 \rangle^{\parallel}_{K^*}$	$\langle \xi^2 \rangle^{\parallel}_{K^*}$	$\langle \xi^2 \rangle^{\parallel}_\phi$
$16^3 \times 32$	0.25(1)(2)	0.035(2)(2)	0.25(1)(2)	0.25(2)(2)	0.037(1)(2)	0.25(1)(2)	0.24(1)(1)
$24^3 \times 64$	0.28(1)(2)	0.036(1)(2)	0.26(1)(2)	0.27(1)(2)	0.043(2)(3)	0.25(2)(2)	0.25(2)(1)

TABLE XII. Comparison to other lattice results (in $\overline{\text{MS}}$ at $\mu = 2$ GeV).

	$\langle\xi^2\rangle_\pi$	$\langle\xi^1\rangle_K$	$\langle\xi^2\rangle_K$	$\langle\xi^1\rangle^{\parallel}_{K^*}$
this work ($24^3 \times 64$)	0.28(1)(2)	0.036(1)(2)	0.26(1)(2)	0.043(2)(3)
QCDSF [23]	0.269(39)	0.0272(5)	0.260(6)	

600 MeV and higher, with two dynamical flavors. For one data point from each collaboration where the pion and kaon masses are comparable, the $\langle\xi^1\rangle_K$ values differ by about 1 standard deviation. These points occur for the smallest values of $m_K^2 - m_\pi^2$ from each collaboration; for larger values the points, and therefore slopes in $m_K^2 - m_\pi^2$, differ. We plan to improve our results in the near future by reducing the systematic uncertainties. We will improve the nonperturbative calculation of the renormalization factors by including the total-derivative mixing term. We will also have an additional lattice spacing, allowing us to estimate the continuum results, including using partially twisted boundary conditions to remove hypercubic lattice artefacts [78,79]. Increased statistics on the $24^3 \times 64$ lattice should also improve our conclusions about finite volume effects.

ACKNOWLEDGMENTS

The calculations reported here were done on the QCDOC computers [48,82,83] at Edinburgh University, Columbia University, and Brookhaven National Laboratory (BNL). The Edinburgh QCDOC system was funded by PPARC JIF Grant No. PPA/J/S/1998/00756 and operated through support from the Universities of Edinburgh, Southampton, and Wales Swansea, and from STFC Grant No. PP/E006965/1. At BNL, the QCDOC computers of the RIKEN-BNL Research Center and the USQCD Collaboration were used. The software used includes CHROMA [54], QDP++, and the CPS QCD codes [50], supported in part by the USDOE SciDAC program; the BAGEL [52] assembler kernel generator for many of the high-performance optimized kernels; and the UKHADRON codes. We thank the University of Southampton for access to the Iridis computer system used in the calculations of the nonperturbative renormalization factors (with support from STFC Grant No. ST/H008888/1). D. B., M. A. D., J. M. F., A. J., T. D. R., and C. T. C. S. acknowledge support from STFC Grant No. ST/G000557/1 and from EU Contract No. MRTN-CT-2006-035482 (Flavianet); R. A. and P. A. B. from STFC Grants No. PP/D000238/1, No. PP/C503154/1, and No. ST/G000522/1; and P. A. B. from RCUK.

[1] G. P. Lepage and S. J. Brodsky, Phys. Rev. D **22**, 2157 (1980).
[2] P. Ball, V. M. Braun, Y. Koike, and K. Tanaka, Nucl. Phys. **B529**, 323 (1998).
[3] V. L. Chernyak, A. R. Zhitnitsky, and V. G. Serbo, JETP Lett. **26**, 594 (1977).
[4] A. V. Efremov and A. V. Radyushkin, Phys. Lett. **94B**, 245 (1980).
[5] G. R. Farrar and D. R. Jackson, Phys. Rev. Lett. **43**, 246 (1979).
[6] M. Beneke, G. Buchalla, M. Neubert, and C. T. Sachrajda, Phys. Rev. Lett. **83**, 1914 (1999).
[7] M. Beneke, G. Buchalla, M. Neubert, and C. T. Sachrajda, Nucl. Phys. **B591**, 313 (2000).
[8] M. Beneke, G. Buchalla, M. Neubert, and C. T. Sachrajda, Nucl. Phys. **B606**, 245 (2001).
[9] C. W. Bauer, S. Fleming, D. Pirjol, and I. W. Stewart, Phys. Rev. D **63**, 114020 (2001).
[10] C. W. Bauer, D. Pirjol, and I. W. Stewart, Phys. Rev. D **65**, 054022 (2002).
[11] C. W. Bauer, S. Fleming, D. Pirjol, I. Z. Rothstein, and I. W. Stewart, Phys. Rev. D **66**, 014017 (2002).
[12] V. M. Braun *et al.*, Phys. Rev. D **68**, 054501 (2003).
[13] C. Allton *et al.* (RBC-UKQCD Collaboration), Phys. Rev. D **78**, 114509 (2008).
[14] S. J. Brodsky, Y. Frishman, G. P. Lepage, and C. T. Sachrajda, Phys. Lett. **91B**, 239 (1980).
[15] V. M. Braun, G. P. Korchemsky, and D. Müller, Prog. Part. Nucl. Phys. **51**, 311 (2003).
[16] P. Ball and M. Boglione, Phys. Rev. D **68**, 094006 (2003).
[17] G. P. Lepage and S. J. Brodsky, Phys. Lett. **87B**, 359 (1979).
[18] A. V. Efremov and A. V. Radyushkin, Theor. Math. Phys. **42**, 97 (1980).
[19] V. N. Gribov and L. N. Lipatov, Sov. J. Nucl. Phys. **15**, 438 (1972).
[20] L. N. Lipatov, Sov. J. Nucl. Phys. **20**, 94 (1975).
[21] Y. L. Dokshitzer, Sov. Phys. JETP **46**, 641 (1977).
[22] G. Altarelli and G. Parisi, Nucl. Phys. **B126**, 298 (1977).
[23] V. M. Braun *et al.*, Phys. Rev. D **74**, 074501 (2006).
[24] A. Khodjamirian, T. Mannel, and M. Melcher, Phys. Rev. D **68**, 114007 (2003).
[25] J. Gronberg *et al.* (CLEO Collaboration), Phys. Rev. D **57**, 33 (1998).
[26] A. P. Bakulev, S. V. Mikhailov, and N. G. Stefanis, Fiz. B **13**, 423 (2004).

[27] V. M. Braun *et al.* (QCDSF-UKQCD Collaboration), Proc. Sci., LAT2007 (2007) 144.
[28] V. M. Braun *et al.* (QCDSF Collaboration), Phys. Rev. D **79**, 034504 (2009).
[29] G. Martinelli and C. T. Sachrajda, Phys. Lett. B **190**, 151 (1987).
[30] D. Daniel, R. Gupta, and D. G. Richards, Phys. Rev. D **43**, 3715 (1991).
[31] L. Del Debbio, M. Di Pierro, A. Dougall, and C. T. Sachrajda (UKQCD Collaboration), Nucl. Phys. B, Proc. Suppl. **83**, 235 (2000).
[32] L. Del Debbio, M. Di Pierro, and A. Dougall, Nucl. Phys. B, Proc. Suppl. **119**, 416 (2003).
[33] M. A. Shifman, A. I. Vainshtein, and V. I. Zakharov, Nucl. Phys. **B147**, 385 (1979).
[34] M. A. Shifman, A. I. Vainshtein, and V. I. Zakharov, Nucl. Phys. **B147**, 448 (1979).
[35] V. L. Chernyak and A. R. Zhitnitsky, Phys. Rep. **112**, 173 (1984).
[36] P. Colangelo and A. Khodjamirian, in *At the Frontier of Particle Physics/Handbook of QCD*, edited by M. Shifman (World Scientific, Singapore, 2001).
[37] A. Khodjamirian, T. Mannel, and M. Melcher, Phys. Rev. D **70**, 094002 (2004).
[38] V. M. Braun and A. Lenz, Phys. Rev. D **70**, 074020 (2004).
[39] P. Ball and R. Zwicky, Phys. Lett. B **633**, 289 (2006).
[40] P. Ball and R. Zwicky, J. High Energy Phys. 02 (2006) 034.
[41] P. A. Boyle *et al.* (UKQCD Collaboration), Phys. Lett. B **641**, 67 (2006).
[42] P. Boyle, M. Donnellan, J. Flynn, A. Juttner, J. Noaki *et al.*, Proc. Sci., LAT2006 (2006) 111 [arXiv:hep-lat/0610025].
[43] P. Hägler, Phys. Rep. **490**, 49 (2010).
[44] M. Göckeler *et al.*, Phys. Rev. D **54**, 5705 (1996).
[45] J. E. Mandula, G. Zweig, and J. Govaerts, Nucl. Phys. **B228**, 91 (1983).
[46] M. A. Clark and A. D. Kennedy, Phys. Rev. Lett. **98**, 051601 (2007).
[47] P. Boyle, D. Chen, N. Christ, M. Clark, S. D. Cohen *et al.*, Nucl. Phys. B, Proc. Suppl. **129–130**, 838 (2004).
[48] P. A. Boyle, C. Jung, and T. Wettig (QCDOC Collaboration), econf C0303241, THIT003 (2003).
[49] P. Boyle, D. Chen, N. Christ, M. Clark, S. D. Cohen *et al.*, Nucl. Phys. B, Proc. Suppl. **140**, 169 (2005).
[50] Columbia Physics System code developed by members of Columbia University, Brookhaven National Laboratory, and UKQCD, http://qcdoc.phys.columbia.edu/cps.html.
[51] P. A. Boyle, Comput. Phys. Commun. **180**, 2739 (2009).
[52] P. A. Boyle, BAGEL assembler generator, http://www.ph.ed.ac.uk/~paboyle/bagel/Bagel.html (2005).
[53] C. Allton *et al.* (RBC and UKQCD Collaborations), Phys. Rev. D **76**, 014504 (2007).
[54] R. G. Edwards and B. Joo (SciDAC Collaboration), Nucl. Phys. B, Proc. Suppl. **140**, 832 (2005).
[55] P. Boyle (UKQCD Collaboration), J. Comput. Phys. **179**, 349 (2002).
[56] C. R. Allton *et al.* (UKQCD Collaboration), Phys. Rev. D **47**, 5128 (1993).
[57] J.-W. Chen and I. W. Stewart, Phys. Rev. Lett. **92**, 202001 (2004).
[58] J.-W. Chen, H.-M. Tsai, and K.-C. Weng, Phys. Rev. D **73**, 054010 (2006).
[59] Y. Aoki, P. Boyle, N. Christ, C. Dawson, M. Donnellan *et al.*, Phys. Rev. D **78**, 054510 (2008).
[60] J. A. Gracey, Nucl. Phys. **B667**, 242 (2003).
[61] J. A. Gracey, J. High Energy Phys. 10 (2006) 040.
[62] M. A. Donnellan *et al.*, Proc. Sci., LAT2007 (2007) 369 [arXiv:0710.0869].
[63] P. A. Boyle, D. Brömmel, M. A. Donnellan, J. M. Flynn, A. Jüttner, and C. T. Sachrajda (RBC and UKQCD Collaborations), Proc. Sci., LAT2008 (2008) 165 [arXiv:0810.1669].
[64] S. Aoki, T. Izubuchi, Y. Kuramashi, and Y. Taniguchi, Phys. Rev. D **59**, 094505 (1999).
[65] S. Aoki, T. Izubuchi, Y. Kuramashi, and Y. Taniguchi, Phys. Rev. D **67**, 094502 (2003).
[66] Y. Iwasaki, Report No. UTHEP-118, 1983.
[67] S. Capitani, Phys. Rev. D **73**, 014505 (2006).
[68] R. Horsley, H. Perlt, P. E. L. Rakow, G. Schierholz, and A. Schiller (QCDSF Collaboration), Phys. Lett. B **628**, 66 (2005).
[69] M. Göckeler *et al.*, Eur. Phys. J. C **48**, 523 (2006).
[70] M. Göckeler *et al.*, Nucl. Phys. **B717**, 304 (2005).
[71] S. Aoki and Y. Kuramashi, Phys. Rev. D **68**, 034507 (2003).
[72] G. Martinelli, C. Pittori, C. T. Sachrajda, M. Testa, and A. Vladikas, Nucl. Phys. **B445**, 81 (1995).
[73] C. Sturm *et al.*, Phys. Rev. D **80**, 014501 (2009).
[74] M. Göckeler *et al.*, Nucl. Phys. **B544**, 699 (1999).
[75] P. Boucaud, F. de Soto, J. Leroy, A. Le Yaouanc, J. Micheli *et al.*, Phys. Lett. B **575**, 256 (2003).
[76] F. de Soto and C. Roiesnel, J. High Energy Phys. 09 (2007) 007.
[77] J. A. Gracey, Nucl. Phys. **B662**, 247 (2003).
[78] R. Arthur and P. Boyle (RBC and UKQCD Collaborations), arXiv:1006.0422.
[79] R. Arthur and P. A. Boyle, Proc. Sci., LATTICE2010 (2010) 244.
[80] K. Nakamura *et al.* (Particle Data Group), J. Phys. G **37**, 075021 (2010).
[81] Y. Aoki (RBC Collaboration), Proc. Sci., LAT2008 (2008) 222 [arXiv:0901.2595].
[82] P. Boyle *et al.*, IBM J. Res. Dev. **49**, 351 (2005).
[83] P. A. Boyle *et al.*, J. Phys. Conf. Ser. **16**, 129 (2005).